Федеральное государственное автономное образовательное учреждение
высшего образования
«Московский физико-технический институт
(государственный университет)»

Факультет биологической и медицинской физики
Кафедра трансляционной и регенеративной медицины

ANGULAR DEPENDENCE CORRECTION OF MATRIXX AND IMPROVEMENT OF THE MEASUREMENT ACCURACY OF IMRT AND VMAT COMPOSITE DOSE VERIFICATION

Выпускная квалификационная работа
(магистерская диссертация)

Направление подготовки: 03.04.01 Прикладные математика и физика

Выполнил:
студент 1112 группы
Петров Пламен Любомиров

_____

Научный руководитель
доктор медицинских наук
Ликарь Юрий Николаевич

_____

Научный консультант :
старший медицинский физик
Отделения лучевой терапии
ННПЦ ДГОИ им. Д. Рогачева
Логинова Анна

_____

Москва 2017

LIST OF ABBREVIATIONS

ADC – analog-to digital converter

CT - computed tomography

DTA - distance-to-agreement

EPID - electronic portal imaging device

IMRT - Intensity-Modulated Radiotherapy

linac - linear accelerator

LUT - look up table (The sets of correction factors are stored in it)

MLC - Multileaf collimator

MU - monitor unit

NTCP - normal tissue complication probability

OD - optical density

QA - Quality Assurance

ROI - region of interest

SCD - source-chamber distance

TCP - tumor control probability

TPS - treatment planning system

VMAT - Volumetric Modulated Arc Therapy

VSM - Virtual Source Model

XVMC - X-ray Voxel Monte Carlo

CONTENTS

INTRODUCTION

The main goal of radiotherapy is to save the patient's life, while maintaining quality of life. For decades it has been known that crucial for achievement of tumor control is delivering a high dose to the tumor, but increasing the radiation dose and irradiated volume, increases the probability of complications. The goal of delivering sufficient dose to the tumor along with minimal dose everywhere else has not been easily approached with the limitations of early technologies. PET, MRI and SPECT imaging allowed to better differentiate the tumor from normal tissues. Precise radiation delivery became possible with the development of techniques such as Intensity Modulated Radiation Therapy (IMRT) and Volumetric Modulated Arc Therapy (VMAT), Image-guided radiation therapy. Advances in the field of radiobiology made it possible to benefit effectively from this possibility.

External beam radiation therapy uses from one field up to a few thousands. As the number of fields increases, several observations were made: The high-dose region becomes more conformal to the target structures, and the dose to the normal tissue decreases but the volume of irradiated tissue covered by peripheral dose increases. Conformal radiotherapy was developed to create dose distribution with a shape that conforms to the target by using beams of various weights, shapes and orientations to the target. Variety conformal delivery techniques are available. With different irradiation techniques different degree of conformation can be achieved. The first conformal therapy was Three-dimensional conformal radiotherapy, based on carefully shaped fixed fields delivered from many directions and 3D treatment planning. Improvements in plan adaptation and optimization resulted in the advent of Intensity Modulated Radiation Therapy (IMRT). In IMRT beams with a complex intensity distribution at a set number of gantry angles are delivered. Volumetric Modulated Arc Therapy (VMAT) was developed to increase patient throughput while maintaining the benefits of IMRT treatments. With VMAT dose rate, beam aperture shape, and the speed of rotation are varied concurrently as the gantry undergoes a single arc.

Radiotherapy treatment relies on the accurate delivery of radiation which should be at least ± 5% of the prescribed dose [1] for most cases, however there is not a single measurement technique or device widely accepted for patient-specific quality assurance for IMRT and VMAT techniques. With the advent of sophisticated radiotherapy techniques, the treatment delivery may require new quality assurance equipment and methods.

Two dimensional arrays are one of the devises used for patient specific quality assurance. Measurements with two dimensional arrays for irradiations at gantry angles other than

those corresponding to normal incidence on the device, have been reported to not always match that calculated by the Treatment Planning System. To use this devices efficiently, sets of angular dependent correction factors have to be created. These correction factors have been derived in variety ways, with several underlying assumptions. Often it is assumed that all detectors have identical response for each angle and that the responses for angles in range 0° — 180° are similar to the responses from 180° — 360°.

IMRT and VMAT are used routinely at the Federal Research and Clinical Center of Pediatric Hematology, Oncology and Immunology Dmitry Rogachev. Currently for patient specific quality assurance purpose at "Dmitry Rogachev" is used a 2D ion chamber array (MatriXX Evolution, IBA Dosimetry).

The goal of my study is to investigate VMAT and IMRT patient-specific quality assurance and to increase the accuracy of quality assurance measurement through the correction of angular dependence of MatriXX Evolution. First the MatriXX Evolution properties would be inspected. The stability of the accelerator dose delivery will be investigated at different gantry angles over a full 360° arc. In order to correct the MatriXX for its strong angular dependence sets of correction factors (LUTs) for 6MV, 10 MV and 15 MV photon beams will be created.

1. Theoretical part

1.1. Tumor control

In planning radiotherapy regimen a risk-versus-benefit approach is taken. Sufficiently high doses can eradicate any and all malignant tumors, in practice the dose that can be administered is limited by the biological consequences for normal tissues that are irradiated along with the tumor. Ideally it will be achieved maximum probability of tumor control that produce acceptable normal tissue damage. As a measure of the efficacy of treatment often is used the ratio of the tumor response for a fixed level of normal-tissue complication, also termed therapeutic ratio [2]. The course of radiation therapy, should be such that as close as possible to the optimal therapeutic ratio is achieved. Figure 1.1 shows examples for "unfavorable" and "optimal" therapeutic ratio. The relationship between delivered dose and the radiation effect is given by a sigmoid curve. Sigmoid curve for tumor control probability (TCP) and for normal tissue complication probability (NTCP). Actual dose-response curves have more variable shape.

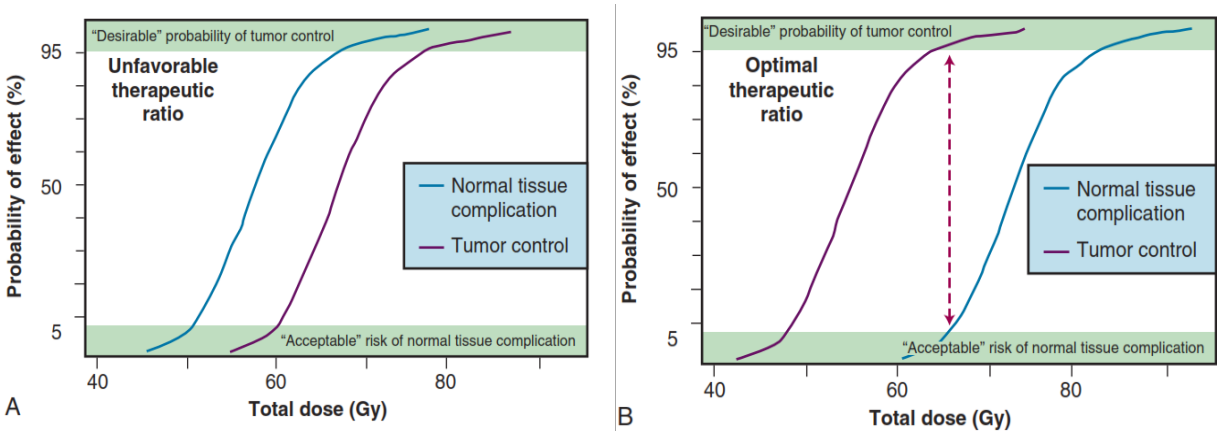

Figure 1.1. *- Therapeutic ratio concept. Tumor control probability (TCP) and for normal tissue complication probability (NTCP) curves.*

Accurate QA procedure to prevent execution of patient plans with "unfavorable" therapeutic ratio is essential for a successful treatment. Dose -response curves are derived from clinical and experimental data. The therapeutic ratio is affected by radiobiological properties of cells. In practice it is difficult to assign a single numerical value to the therapeutic ratio. Biological models TCP and NTCP are crucial for the determination of the plan with best therapeutic ratio from many. Tumor control is achieved only when all neoplastic stem cells causing tumor growth are killed in the sense that that they lose their reproductive integrity [3]. Before succumbing to death in the traditional sense some cells may undergo a few additional mitoses. They are responsible for the preservation of the tissue size and function. The cells within the volume of a tumor may be: neoplastic stem cells, cells that have started irreversible process of

differentiation and normal host cells. The neoplastic stem cells are causing tumor growth. If there is a mixture of sensitive and more resistant neoplastic stem cells, then the sensitive subgroup will have a dose–response curve that lies to the left of that for the more resistant tumors. The overall dose–response curve will, therefore, be a composite of steep curves at different points on the dose scale, and it will be flatter than any single one of them.

After irradiation the most probable mechanism of death is mitotic death, the cell dies while attempting to divide. Another possible mechanism is apoptosis. Following apoptosis, the type of inflammatory response, tissue destruction, and disorganization which is typically observed following necrosis is absent, because apoptotic cells are phagocytized by neighboring cells. Exposure of biological material to radiation leads to ionization and excitation of its atoms [2]. The molecules which include such atoms in their structure tend to fall apart and free radicals are produced. Most free radicals within the cell are result of the radiolysis of water, for example hydroxyl radical. The highly reactive free radicals react with nearby molecules and inflict chemical damage to them. All cell components can be damaged in this way, however whether the damage will be lethal to the cell depends upon a number of factors, for instance the number of damaged molecules and their importance to the cell. Furthermore, the effect a death of a cell will have to corresponding tissue or organ depends upon its importance to them. When the radiation reacts directly with the critical target, the mechanism is referred to as "direct radiation action" and when the critical target is damaged by free radicals due to radiation, is referred to as" indirect radiation action". The amount of oxygen within a cell has a strong influence on the biological effect of ionizing radiation. Molecular oxygen, due to its two unpaired electrons readily reacts with free radicals, increasing the probability of damage occurring in DNA by the indirect process. DNA is an important cellular macromolecule. It is a very long double-helix molecule, which consist repeated sequence of bases, and every chromosome has approximately 200 million bases. Genes formed by groups of bases contain instructions for proteins and hence for the cellular function. Cells have repair enzymes continually monitoring the integrity of the DNA, recognizing damage, and repairing it and often there is duplication of genes, however a serious risk exists that damaged DNA will lead to the modification or loss of genes which will lead to a loss of specific function.

A cell survival curve describes the relationship between the radiation dose and the surviving fraction of cells. Figure 1.2 shows a cell survival curve for mammalian cells, with radiation dose plotted on the linear horizontal axis and surviving fraction plotted on the logarithmic vertical axis [4]. Each point on the graph represent the fraction of survived cells after delivery of single acute dose of the specified radiation. Cell survival curves are often described by the linear quadratic model.

$$S(D) = e^{-\alpha D - \beta D^2}$$

where α is describing the initial slope of the curve, β is describing the quadratic component of cell killing and *S(D)* is the fraction of cells surviving a dose *D*. Cell killing at clinically realistic doses per fraction is dominated by the linear component of the cell-survival curve.

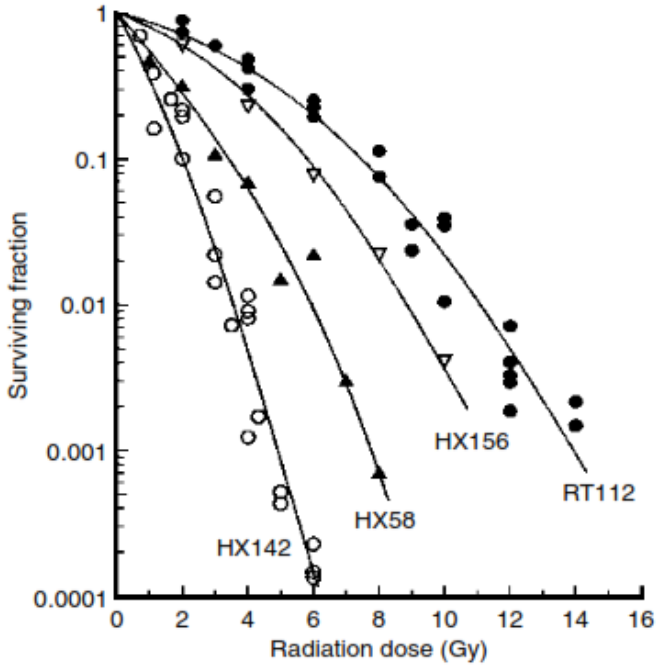

Figure 1.2. *- Cell survival curves for four human tumor cell lines irradiated at high dose rate. HX142 neuroblastoma; HX58 pancreatic; HX156 cervix; RT112 bladder carcinoma.*

The linear-quadratic equation has been derived from two different sorts of observations. It has been proposed [5] that a radiation-induced lethal lesion is produced by the interaction of two sublesions. The term α gives the probability that a single event will produce the sublesions and β is the probability that two separate events will produce the sublesions. The same equation has been derived [6] based on a the assumption, that a double strand break in DNA is a lethal lesion and also that a lethal lesion could be produced by a single energy deposition which involves both DNA strands or by two separate events, each involving just one of the strands.

The main purpose of clonogenic cell survival studies is to understand and make predictions about, the way tumor will response to particular therapy. Incomplete treatment of a tumor result in a temporary phase of tumor regression, due to the death of cells, followed by tumor recurrence, due to repopulation by surviving clonogenic cells [3]. Delivering the dose in fractions separated apart by a few hours or more, gives the cell time, during which the cell can repair its damaged structures and allowing a higher total dose to the normal tissue.

Radiation effects are always more severe or more likely to occur as the radiation dose is increased. They also become more frequent as the size of the radiation field is increased. This

is called the volume effect. Related to this is the question of which normal structures are contained within the radiation field, as enlargement of the field may result in the inclusion of a structure that otherwise would not have been irradiated. TCP is influenced by dose nonuniformity, furthermore different organs have different tolerance dose at which a given level of late radiation morbidity can be expected. Assuming constant clonogenic cell density [7] showed that inhomogeneities in the target dose distribution and uncertainties in the absolute absorbed dose lead to decrease of TCP. In reality colonogenic cell density is not constant and ideally to regions with higher density higher doses would be delivered. Only in the tissues directly irradiated by the primary beam(s) anticancer effect is seen. The choice of beam arrangements has to ensure that the prescribed dose is actually absorbed in the tissue volume that contains each and every neoplastic stem cell, taking into consideration the net effect of all possible geometrical variations [3].Example of conformal plan is shown on figure 1.3.

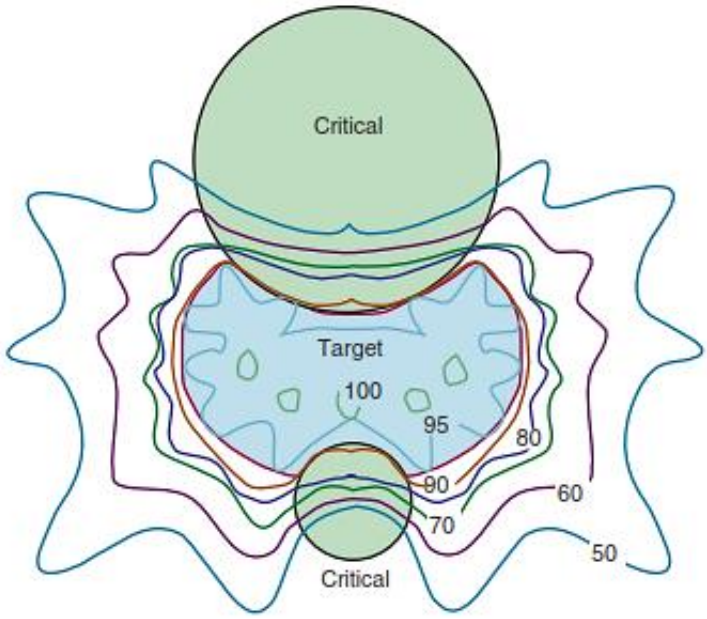

Figure 1.3. *- Example of intensity-modulated plan for a target between critical structures.*

With technologies such as conformal radiotherapy, IMRT and VMAT, the delivered dose to critical structures can be limited substantially while still irradiating the tumor in its entirety. However this is possible only if the therapeutic absorbed dose is delivered to the patient reliably and reproducibly every day of the treatment course.

1.2. Dosimetry

Essential to the success of radiotherapy is the accurate determination of absorbed dose. Difference of a few percent in the delivered dose may lead to underdosage or overdosage. The determination of the absorbed dose distribution in the patient includes many steps. Numerous specifications of the radiation field, through measurements with a detector are crucial to this

process. Mapping the complete dose distribution includes measurements at many points of interest in a phantom. The detector measures dose from a quantity of charge, film blackening, etc., thus a calibration factor to convert from such quantities to dose is necessary. Furthermore, the presence of the phantom and the detector will influence the radiation field. Oftentimes the dose in the absence of phantom and the detector, is of interest, which requires another conversion.

1.2.1. Basic dosimetry concepts

Vital dosimetry concepts and principles will be described here:

- **The particle fluence** *F* is the number of particles *dN* striking a finite sphere surrounding point *P*. Reducing the sphere to infinitesimal size at *P*, the fluence *F* is given by [3].

$$F = \frac{dN}{dA} \tag{1.1}$$

where *dN* is the number of particles incident on a sphere of cross-sectional area *dA.*
The unit of particle fluence is m^{-2}.

- **Energy fluence** Ψ is the expectation value of the total energy *R* (excluding rest mass energy) carried by all *N* particles in a infiniteniosly small sphere [4] with cross-section *A.*

$$\Psi = \frac{dR}{dA} \tag{1.2}$$

The unit of energy fluence is J/m^2.

- **Planar particle fluence** is the number of particles crossing a plane per unit area [8]. The particle fluence rate $\dot{F}$ and energy fluence rate Ψ (intensity) are defined as [3]:

$$\dot{F} = \frac{dF}{dt} \tag{1.3}$$

and

$$\Psi = \frac{\Psi}{dt} \tag{1.4}$$

where *dt* is time interval.

- **KERMA** (stands for kinetic energy released per unit mass) *K*, is the sum of the initial kinetic energies, dE_{tr} of all the charged ionizing particles liberated by uncharged ionizing particles in a material of mass *dm* [3]:

$$K = \frac{dE_{tr}}{dm} \tag{1.5}$$

The unit of KERMA is J/kg, also called gray – Gy.

The KERMA has two components:

a) Collision kerma, K_{col} –The energy loss of secondary electrons that dissipate their energy as ionization in the medium.

b) Radiative kerma K_{rad} –The energy loss due to radiative photons as the secondary charged particles slowdown in the medium.

$$K = K_{col} + K_{rad}$$

The ratio of radiative kerma and the total kerma is called also radiative fraction g and the collision kerma can be expressed as:

$$K_{col} = (1-g)K \tag{1.6}$$

In the condition of charged particle equilibrium the absorbed dose and the collision kerma are equal.

$$K_{col} = D$$

Absorbed dose is the quotient of $\bar{d}\varepsilon$ by dm, where $\bar{d}\varepsilon$ is the mean energy imparted by ionizing radiation to matter of mass dm [3]:

$$D = \frac{\bar{\mathrm{d}}\varepsilon}{\mathrm{dm}} \tag{1.7}$$

The unit of absorbed dose is Gy

Exposure is the quotient of dQ by dm where dQ is the absolute value of the total charge of the ions of one sign produced in air when all the electrons liberated by photons in air of mass dm are completely stopped in air [8], thus the unit of exposure is C/kg.

$$X = \frac{dQ}{dm} \tag{1.8}$$

The exposure can be measured directly with ionization chamber, but often the interest lies in knowing the absorbed dose or other dosimetric quantities.

After the basic dosimetric quantities are defined the relationships between them can be established. The relationship between exposure and collision kerma is given by [8]:

$$X\frac{\bar{W}_{med}}{e} = K_{col,med} \tag{1.9}$$

where $\frac{\bar{W}_{med}}{e}$ is the quotient of the average energy expended in air per ion pair formed in the medium and the elementary charge. The current best estimate for the average value of $\bar{W}_{med}$ in air is 33.97 eV/ion pair.

The relationship between the total kerma and exposure is [8]

$$K_{col,med} = X\frac{\bar{W}_{med}}{e}\frac{1}{1-g} \tag{1.10}$$

Device that provides a reading which represents the average absorbed dose deposited in its sensitive volume by ionizing radiation or possess at least one physical property that is a function of the measured dosimetric quantity, after a proper calibration is named dosimeter [8].

Bragg-Gray cavity theory provides relation between the absorbed dose in the dosimeter and the absorbed dose in the medium surrounding it. The theory is applicable under the following conditions [8]:

- The cavity dimensions must be small when compared to the range of the charged particles incident on it, if this condition is not met the presence of the cavity will perturb the fluence of charged particles in the medium. Given that there is charged particle equilibrium or transient charged particle equilibrium, the electron fluences in the cavity and the surrounding medium are the same (there is always at least a small perturbation of the fluence).
- The photon interactions in the cavity must be negligible because it is assumed that the absorbed dose in the cavity must be deposited solely by charged particles crossing it. Bragg-Gray cavity theory gives the following relationship between the absorbed dose in the cavity D_{cav} and the medium surrounding it $D_{med.}$

$$D\ med, cav = \left(\frac{\bar{S}}{\rho}\right) med, cav \tag{1.11}$$

where $\left(\frac{\bar{S}}{\rho}\right) med, cav$ is the ratio of the average unrestricted mass collision stopping powers of the medium and the cavity.

In Bragg–Gray theory it is assumed that charged particles lose energy by a large number of extremely small energy-loss events. Spencer and Attix extended of the Bragg–Gray cavity theory [8], by taking into account the secondary electrons generated as a result of hard collisions of the primary electrons in the cavity. In their theory the same assumption regarding the conditions are made, but now they also apply to the secondary particle fluence. All the electrons under a cutoff energy Δ are slow electrons that deposit their energy locally and all with energy above Δ are considered part of the electron spectrum, this way all energy losses above Δ are considered to escape entirely. The cutoff energy Δ should be set equal to the energy of electrons with a range just sufficient to cross the cavity. The energy deposition is calculated as the product of the restricted collision stopping power with threshold Δ $L_\Delta(E_k)/\rho$ and the fast electron fluence Φ^{e-e}_{med,E_k} ranging in energy from Δ to E.

The dose to the medium and the dose in the cavity are related by the ratio of the mean restricted mass collision stopping powers of the medium to that of the cavity $s_{med,cav}$:

$$\frac{D_{med}}{D_{cav}} = s_{med,cav}$$

$$s_{med,cav} = \frac{\int_\Delta^{E_{k0}} \Phi^{e-e}_{med,E_k}(E_k)\left(\frac{L_{\Delta,med}(E_k)}{\rho}\right) d(E_k) + \Phi^{e-e}_{med,E_k}(\Delta)\frac{S_{med}(\Delta)}{\rho}}{\int_\Delta^{E_{k0}} \Phi^{e-e}_{med,E_k}(E_k)\left(\frac{L_{\Delta,cav}(E_k)}{\rho}\right) d(E_k) + \Phi^{e-e}_{med,E_k}(\Delta)\frac{S_{cav}(\Delta)}{\rho}} \tag{1.12}$$

The terms $\Phi_{med,E_k}^{e-e}(\Delta)\frac{S_{med}(\Delta)}{\rho}$ and $\Phi_{med,E_k}^{e-e}(\Delta)\frac{S_{cav}(\Delta)}{\rho}$ are in the expression, to include part of the energy deposited by electrons with initial kinetic energies between Δ and 2Δ and $\frac{S_{med}(\Delta)}{\rho}$ is the unrestricted collision stopping powers, it is used, because the maximum energy transfer for an electron with energy less than 2Δ is less than Δ [8], E_{k0} is the initial electron kinetic energy.

The dosimeter cavity usually contain gas, because it is relatively simple to collect the charges released in a gaseous medium, however, it could contain liquid or solid medium. The relationship of the absorbed dose in the cavity to the absorbed dose in the surrounding medium is given by cavity theory. If the range of charged particles is much larger than the cavity dimensions, the cavity is regarded as small. If the range of charged particles is much smaller than the cavity dimensions, the cavity is regarded as large. If neither is the case the cavity is "intermediate" [8]. The medium that serves as build up around the cavity could be the walls or the phantom in which it is used, if the range of the secondary electrons in the wall is much longer than its thicknesses. In the second case the wall is taken into account, with the inclusion of perturbation factor in the dose calculation, because the dose due to secondary electrons generated in the wall is much smaller, than the dose due to electrons generated in the cavity.

1.2.2. Accurate dosimetry with ionization chambers

Ionization chambers are often used in radiotherapy clinics for absolute and relative dose measurements. A 2D array of ionization chambers and Farmar chamber are used in this work. The sensitive volume of the ionization chamber is usually air at atmospheric pressure and the radiation causes the formation of ions and electrons. Between 2 electrodes high, but insufficient to crate gas multiplication voltage is applied, and the charges are moving towards the electrodes of the opposite sign. The central collecting electrode collects the charge, and the current due to collected charge can be measured [3]. As the voltage increases, the ion recombination decreases, more charged particles are collected and when all pairs formed are collected, the signal reaches saturation. The electric field between the electrodes can create a leakage current in the insulator that leads to higher measured signal. To reduce the leakage current, there is a high quality insulator separating the wall from the collecting electrode and guard electrode that intercepts the leakage current and redirect it to the ground. The guard electrode also improves the field uniformity in the chamber. The chamber current is passed to a high gain, negative feedback, operational amplifier with a capacitor or resistor in the feedback loop and after the amplifier measured with an electrometer.

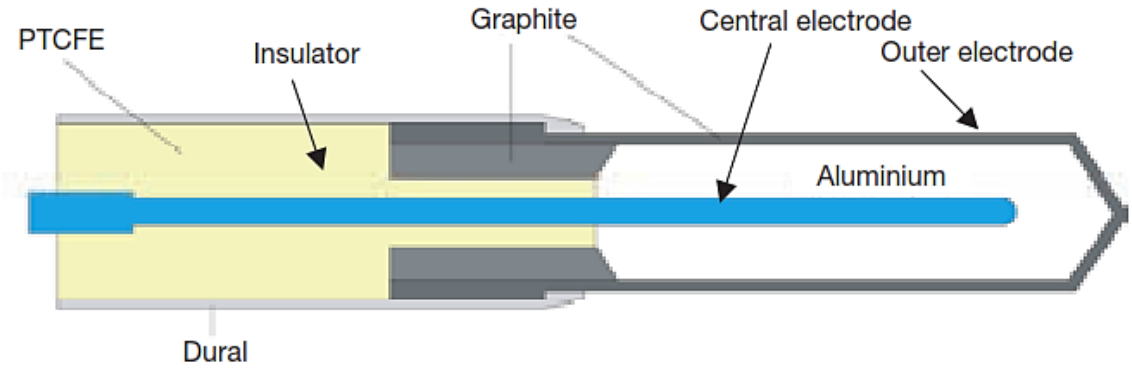

Figure 1.4. *- Cylindrical Farmer ionization chamber design.*

If the presence of the chamber does not perturb the photon fluence and the absorbed dose is the same as the collision kerma, then the dose in the cavity can be calculated by the product of the charge produced in the cavity Q per unit mass m of the gas in the cavity and $\bar{W}_{gas}$.

$$D_{gas} = \frac{Q}{m}\left(\frac{\bar{W}_{gas}}{e}\right) \tag{1.13}$$

The secondary electrons crossing the cavity may be result primarily of the interactions in the wall or the medium surrounding the wall. This depends on the ratio of the wall thickness compared to the range of secondary electrons in the wall itself.

There are two cases for practical purposes:

A) The wall is thick enough to ensure that the electrons arise solely in the wall (the electrons from the medium can be neglected or taken in account by introducing a perturbation factor)

According to equations (1.12) and (1.13) the dose in the medium can be calculated as:

$$D_{med} = D_{wall}\left(\frac{\bar{\mu}}{e}\right)_{med,wal} = D_{gas}s_{wall,gas}\left(\frac{\bar{\mu}}{e}\right)_{med,wal}$$

$$D_{med} = \frac{Q}{m}\left(\frac{\bar{W}_{gas}}{e}\right)s_{wall,gas}\left(\frac{\bar{\mu}}{e}\right)_{med,wal} \tag{1.14}$$

B) The wall is thin enough to ensure that the electrons arise primarily in the medium.

$$D_{med} = \frac{Q}{m}\left(\frac{\bar{W}_{gas}}{e}\right)s_{med,gas} \tag{1.15}$$

There are several perturbation factors [3], [8], [9] that have to be included in eq. (1.13):

1. Wall correction factor.

   Factor that takes in to account the electrons that arise from the wall $p_{wall.}$
2. Factor to take into account the change in the mass of air in the chamber volume $p_{mass.}$
3. Correction factor for the changes in the air mass within the cavity $p_{T,P.}$

The mass of the air in the chamber is proportional to its density and the density is a function of the pressure, temperature and humidity. It is a common practice for the correction

factor to be given to a pressure P_0=101.325 kPa, temperature T_0=20˚C and it is valid for humidity in the range 20% to 70%. In the user beam, the correction factor is given by:

$$p_{T,P} = \frac{(273.2 + T)}{(273.2 + T_0)} \frac{P_0}{P} \tag{1.16}$$

4. Correction factor for displacement of the effective measurement point $p_{eff.}$

The dose may differ by a few percent in different points of the chamber (if the radiation field gradient is not negligible compared to the detector's volume) and the detector is displacing part of the volume of the medium, thus the attenuation and the scatter are reduced. The net result is an increase in the chamber signal. To account for that a displacement factor, p_{diss} is applied or the effective point of measurement can be moved $p_{eff.}$ The value of the displacement factor depends on the: radiation quality, physical dimensions of the air cavity in the direction of the beam, depth of measurement. For cylindrical chambers the recommended shift is 0.5r.

5. Correction factor for the central electrode p_{cell}

It accounts for the lack of air-equivalence of the central electrode.

6. Electron fluence perturbation correction factor p_{cav}

The electron fluence is distorted due to heterogeneity in the medium. The electron beam angular distribution broadens with depth due to scattering. In a region where the density of the medium, compared to regions with higher density, the broadening will be to a lesser degree, thus more electrons are scattered into a low density region then out of it. In the context of measurements with ionization chamber, the gas in the ionization chamber is a low density medium and a perturbation factor should be introduced to account for the rise of the photon fluence inside the chamber cavity p_{cav}.

7. Correction factor for ion recombination $p_{s.}$

The recombination of ions within the air cavity leads to incomplete collection of charge. The effect depend on the applied polarizing voltage and on the chamber geometry.

The recombination of ions formed by a single ionizing particle track is called initial recombination and the recombination of ions formed by different tracks is called general recombination. The dose rate can affect the general recombination, but it doesn't affect the initial recombination. The following approximate empirical relationships characterize the recombination as a function of the measured charge q and the polarizing voltage V.

The initial recombination is described by the equation:

$$\frac{1}{q} = \frac{1}{q_0} + \frac{constant}{V} \tag{1.17}$$

The general is described by the equation:

$$\frac{1}{q} = \frac{1}{q_0} + \frac{constant}{V^2} \tag{1.18}$$

A method to estimate the recombination, that assumes a linear dependence between the reciprocal values of the collected charge and the polarizing voltage has been described [10], [11].The collected charge has to be measured at the normal operating voltage V_1 and at lower voltage V_2 in the same irradiation conditions.

The following equation can be used for the calculation of the correction factor p_s:

$$p_s = a_0 + a_1 \frac{Q_1}{Q_2} + a_2 \left(\frac{Q_1}{Q_2}\right)^2 \tag{1.19}$$

where Q_1 and Q_2 are the collected charges respectively at voltages V_1 and V_2, and the coefficients a_0 , a_1 and a_2 are coefficients given as a function of V_1/V_2.

8. Correction factor for polarity effect p_{pol}

The chamber reading may yield different values when its polarity is reversed, this effect is named polarity effect. The true chamber reading is taken to be the mean of the absolute values of readings taken at both polarities. Usually a single polarizing potential and polarity are normally employed in the routine use of an ionization chamber. In order to take into account the polarity effect a correction factor is needed and it is calculated according to the following equation:

$$p_{pol} = \frac{|M_-||M_+|}{2M} \tag{1.20}$$

where M_+ and M_- are the obtained electrometer readings at each polarity and M is the reading with the polarity used routinely.

Applying all factors to formula (13) the expression for the absorbed dose becomes:

$$D_{med} = \frac{Q}{m}\left(\frac{\overline{W}_{gas}}{e}\right) s_{med,gas} p_{fl} p_{dis} p_{wall} p_{diss} p_{T,P} p_{pol} p_s p_{cav} \tag{1.21}$$

1.2.3. Film dosimeters

Film can be used as a radiation detector, a relative dosimeter, a display device and an archival medium [3]. The degree of film blackening correlates with the so called light opacity. Light opacity is a measure of the attenuating properties of the film. To determine it a beam of light is passed through the irradiated film and light intensity I_0 is measured, in the same conditions light intensity I is measured without the film. The $\log_{10}$ of light opacity is also called optical density OD. OD is linear function of fluence, hence also linear function of dose, but emulsions are linear over a limited dose range.

$$OD = log_{10} \frac{I_0}{I}$$

The responses of different films depend on daily fluctuations in the relative chemical components in the developer, the radiation energy and other parameters. Therefore, prior to the usage of each film this dependence must be established. It is represented as a curve on a coordinate system with OD on one axis and dose on the other. This curve is named sensitometric or characteristic curve. Optical density can be measured with film densitometers, laser densitometers and automatic film scanners. Unirradiated film would exhibit a background density as do irradiated film, this is why unirradiated film is used to set the zero read. Radiographic films are used as dosimeters.

Radiographic film consists of a thin plastic with small radiation sensitive silver-halide crystals (AgBr) suspended in gelatin emulsion coated with a polyester base. The latent image is formed, due to the ionization of AgBr grains by radiation interactions. After that, for the formed image to be visible (film blackening), it should be processed by chemical amplification.

Radiochromic films are nearly tissue equivalent, relatively insensitive to visible light, less sensitive to spectral hardening, don't need chemical processing and they are stable at high temperatures. Ionizing radiation and ultraviolet light cause forming or polymerization processes in the film, thus its color changes. Irradiated film exhibits absorption bands at wavelengths 610 nm and 670 nm. The film reading device can be a He–Ne laser scanning densitometer, or a regular transmission flat-bed-scanner [12]. Radiochromic films have better energy characteristics (for photons of energy less than 25kV) and also are dose rate independent.

1.3. Linear accelerators

Linear accelerator (linac), designed for medical purposes accelerate electrons to kinetic energies up to 25 MeV, by synchronized radio-frequency electromagnetic fields in the range 1 GHz to 2856 MHz. The electrons are moving linearly through the same potential differences several times in structures called accelerating waveguides. Waveguides can reduce the speed of electromagnetic waves, which allows to be achieved the necessary frequencies. They are made of a long cylindrical tube, which contains a series of circular baffles. In the accelerator the electrons are focused onto thick material with high atomic number and as the electrons are stopped, they generate bremsstrahlung radiation, which is largely forward directed at megavoltage energies. Different types of linacs are used in radiotherapy. A typical one provides 6 and 18 MeV photons and several electron energies in the range 6MeV to 22MeV.

The linac has five major sections: Gantry, Gantry stand or support, Modulator cabinet, Patient support assembly, Control console [3]. A schematic diagram of a typical modern linac and relationships among its components is shown on Fig 1.5.

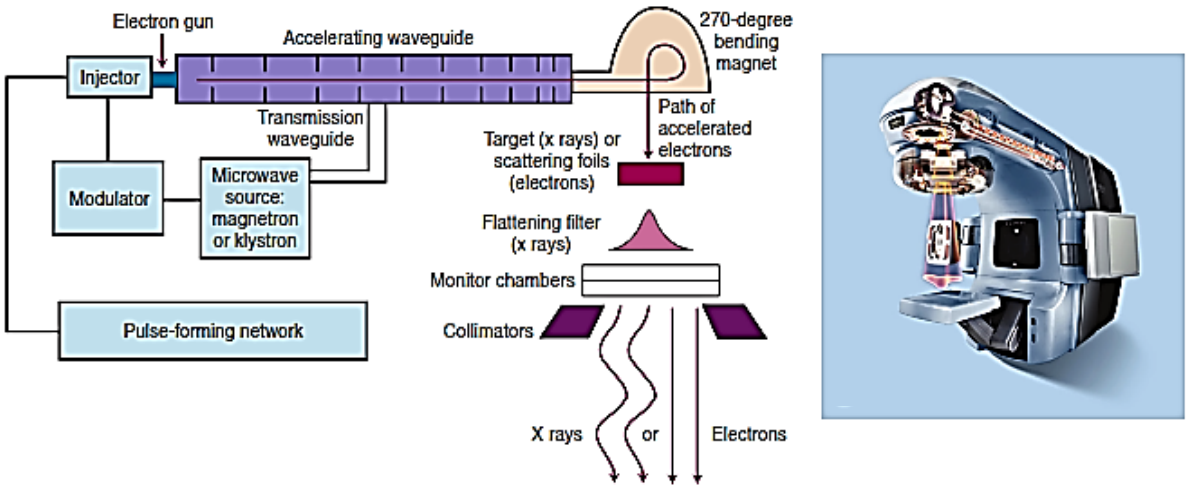

Figure 1.5. *- Medical linac design.*

A heated cathode is emitting electrons, which in their path to the anode are influenced by pulsed electrostatic fields, which results in changes in the electron acceleration. The electrons pass through a hole in an anode, and form bunches a few centimeters apart which go in the waveguide. Pulsed modulator supplies the radio frequency power source and the injection system with the required high voltage, high current and short duration pulses. The radiofrequency power sources for medical accelerators are usually magnetrons for low and medium energy machines and klystrons for high energy machines.

The waveguides are made of metal and have a circular or rectangular cross-section that is evacuated or gas-filled. Corrugations in accelerator waveguides are used to slow up the waves, this makes the crests of the microwave electric field approximately synchronous with the flowing bunches of electrons and the electron bunch is accelerated forward.

The electron beam must be kept directionally as close as possible to the central axis of the guide, because if not the beam current will be reduced and also the guide structure could be damaged. The beam is steered radially and transversely by mounting external solenoidal focus and centering coils at critical points along the guide. Misalignment would cause the beam to strike the target at the wrong angle, which would affect the x-ray beam uniformity and possibly the beam energy. The accelerating waveguide can be mounted with its axis parallel to the central axis of the radiation beam, but for linacs with x-ray energies above 6 MeV this is impractical, because of their long waveguide. The accelerating guide is mounted at approximately right angle with respect to the direction of the radiation beam for this machines, because of that bent beam design becomes essential for them.

A magnet system bends the beam through a net angle of approximately 90˚ or 270˚ onto the x-ray target, electron output window, electron scattering foils, or electron scanning magnet. Such an array of magnets and drift spaces is termed the beam transport system.

The trajectory of every electron as it passes through the bending system dependents on the energy, so narrow energy spreads of the electrons has to be accomplished in order to minimize distortions in flatness of radiation fields, however very narrow energy spread is difficult to achieve. Due to changes in mean energy of the energy spectrum, linear accelerators could employ a bend system where electrons with different energies exit at the same point in the same directions (chromatic system).The advantage of non-achromatic bending systems is that the correct electron energy is ensured by the magnet, while in achromatic it must be monitored and if needed corrected.

Production of x-ray and electron treatment beams for radiotherapy originates in the radiation head. The radiation head is the structure from which the useful treatment beam emerges. Its design strongly influences the characteristics of both the x-ray and electron treatment beams. The head provides a number of beam-shaping, localizing, and monitoring devices. They include a bending magnet if used, fixed shielding, the x-ray target, flattening filter, and a series of single or dual electron scattering foils, usually mounted on a large carousel, and large movable collimator jaws. Included also is a field defining light and an optical distance indicator together with a large diameter, parallel plate, transmission type ionization chamber assembly for monitoring of the full field for control, and interlocking.

The lower portion of the radiation head contains the collimator jaws. The radiation head rotation and collimator jaw movements are usually motor driven and controlled from a cable-connected hand pendant, which controls the speed and direction of gantry rotation and couch movements. It controls also the field-defining together with room and laser patient positioning lights.

Clinical photon beams are generated when a high energy electron beam strikes a target, due to bremsstrahlung process. The bremsstrahlung beam emerging from the target has energy, fluence and angular distributions. These distributions are modified in important ways by the flattening filter. Flattening filters may absorb 50% - 90% of the central axis photon intensity. They, as well as wedge filters, increase scatter, most noticeably outside the geometric confines of the beam. Flattening an x-ray field involves a compromise between penetrability, uniformity and output, in order to achieve uniform small and large fields over a range of depths. Modern linac has energy interlocks that place limits constraints on field unflatness. An angular or a lateral displacement of the beam on the target produces unflattened distributions. The changing earth's magnetic field encountered in gantry rotation may also have an effect. The heavy iron frame cast in the floor used for mounting the linac can produce significant distortions in the earth's field and changes in fringing fields of bend and solenoid magnets as a function of gantry angle of rotation.

Frequent symmetry, dose monitor, and beam energy checks of linac treatment unit must be performed. X-ray output constancy check at different gantry angles was performed in this work. The beam must be shaped so that it irradiates only the cancer cells, this is achieved with collimator devices. The treatment head provides treatment beam collimators. Circular primary collimator, and an adjustable secondary collimator, which is also termed the beam limiting device or "jaws". The primary beam collimator defines the maximum angular spread of the x-ray beam. The adjustable collimators consist of four blocks, two forming the upper and two forming the lower jaws of the collimator. Their defining edges often traverse arcs, or approximate arcs, such that their inner faces are approximately tangential to the radiation beam emanating from the x-ray target thereby reducing penumbra. They define the size of the x-ray treatment field and act in combination with the electron applicator to produce a properly shaped electron treatment field dose distribution.

For some therapy techniques, independent motion of the jaws of one or both pairs is desirable to provide asymmetric rectangular fields. Independent jaw motion is accomplished by uncoupling the symmetrical motion of a pair of jaws and independently positioning each jaw with one jaw edge left on axis for the half-blocked field. Both jaws may also be independently positioned, allowing one jaw of the pair to cross the central axis, to define fields where both field edges are on one side of the central axis. Dual independent collimators, allowing independent motion of all four jaws, provide additional flexibility in blocking offset field edges. However, this necessitates very large jaws and a large secondary collimator diameter in order to shield all areas subtended by the primary collimator. Multileaf x-ray collimators (MLC) have been developed to closely encompass irregularly shaped tumors. This collimator system is made of up to 80 pairs of metal leaves that can move independently, example for beam definition via MLC is shown on fig. 1.6. They can be rapidly set under computer control and can be programmed to follow the changing tumor outline.

Effective and safe radiation therapy requires the performance characteristics of radiation treatment beams to remain constant during each individual treatment, as well as during a series of treatments extended over long periods of time. These characteristics stability will depend on the design and construction of mechanical, electrical, electronic, and ancillary systems of the treatment unit.

The dose monitoring system incorporates a transmission ionization chamber to monitor the beam uniformity, energy, radiation dose and dose rate. This chamber is located in the linac head. The chamber is calibrated is such way that dose of 1 cGy delivered at a reference point in reference conditions and geometry (typically in a water phantom at 100 cm for an unwaged

10 cm x10 cm field at the depth of maximum depth-dose on the central beam axis) corresponds to measurement of 1 monitor unit (MU), by the chamber.

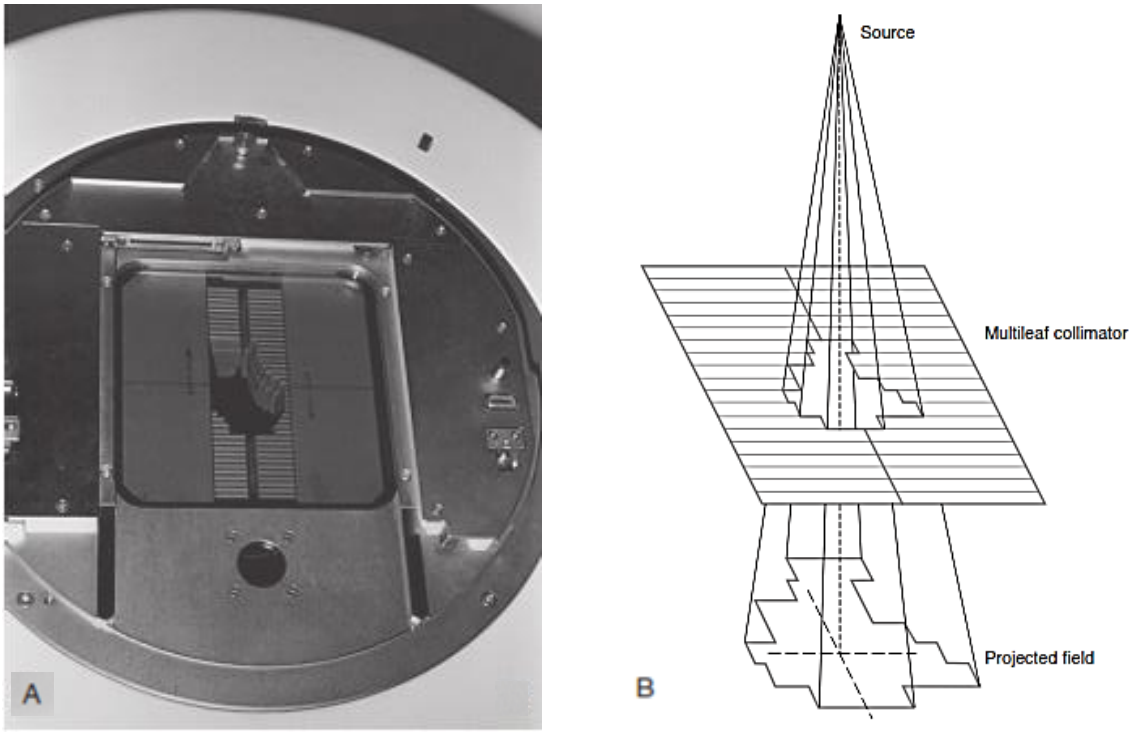

Figure 1.6. *- Multileaf collimator.* ***A****. 80-leaf collimator for Varian 2100C linac.* ***B.*** *Beam definition scheme*

During dose delivery when a preset number of MUs has been reached, the linac shuts down. Contemporary linacs employ two separately sealed ionization chambers with independent biasing power supplies and readout electrometers. The secondary chamber will terminate the irradiation, if the primary chamber fails during patient treatment. The resultant electrical signals from the chamber are also used in automatic feedback circuits to steer the electron beam through the accelerator and bending magnet onto the target (or scattered) in order to ensure treatment beam flatness and symmetry. A treatment beam of x-rays or electrons contains contaminants, both inside and outside the useful beam intended to encompass the tumor. These contaminants are electrons and photons as well as neutrons.

1.4. Dose calculation algorithms utilized in external beam photon radiation therapy

The dose calculation algorithms purpose is to predict the dose distribution in the patient, the treatment plan must be changed until an acceptable distribution is achieved. The dose calculation has to be done relatively fast and yield accurate results. However, increasing the accuracy of the calculation leads to longer calculation time. The choice of the dose algorithm is based on the necessary accuracy. The anatomy of each individual patient and the clinical beam characteristics have to be considered when calculating the dose distribution. Usually the data

for the patient anatomy is derived via computed tomography (CT), then represented in a 3D matrix and combined with the beam data, which unfortunately in practice have to be simplified and obviously this leads to decreasing in accuracy.

There is no single classification methodology regarding dose calculation algorithms, and different suggestions have been made. One of them is do classify them, [13] based on the way integration or superposition of elementary kernels throughout the patient volume is done.

When the algorithm doesn't utilize integration it is referred to as the broad-beam approach. The dose distribution under this approach can be calculated using tabulated beam data for a number of beams or beam generating functions for simple beams. The tabulated beam data is derived from measurements under reference conditions and is interpolated by the treatment planning system (TPS) during calculation. The beam generating functions model the beam depth-dose and profile characteristics. Usually the dose is calculated by multiplication of two analytical functions. Beam generating function gives satisfying results only for limited range of energies and field sizes [3]. The broad-beam approach requires many corrections and doesn't give satisfactory results when greater accuracy is required or the situation is more complex, however it yields results quickly.

The superposition approach takes into account the primary photons and the secondary particles separately [3]. The dose at every point is calculated by summing the energy contributions from the scattering volume elements in the medium to the dose at that point.

The calculation can be speeded up, in case that simplifying assumptions are made. However, these assumptions may cause insufficient accuracy.

The fundamental equations that describes the transport of ionizing radiation in matter, can be solved numerically by the Monte Carlo method, if the scattering and absorption cross-sections are known. Monte Carlo simulation was used to calculate dose distributions in the MatriXX detector. The ionizing radiation is described by modelling many independent particle history (the chain of events that happens to each individual particle that is modelled) and the statistics of the samples is analyzed to determine the cumulative behavior of many ionizing particles [14]. The initial energy and direction of the particle are randomly sampled, according to their probability. The interaction of the radiation with matter is also randomly chosen according to the probability of interaction and the nature of that interaction. Any secondary radiation that is created from the interactions is then followed similarly, in order to describe the entire radiation effect. Only the fundamentals of the methodology used to transfer ionizing particles in the energy range of radiation therapy is represented here, because this is quite complex.

The probability *p(s)* that a photon of energy *E* interacts after path length *s* with the medium is given by the attenuation law:

$$p(s)ds = \mu(E)^{-\mu(E)s}ds \tag{1.22}$$

where $\mu(E)$ is linear attenuation coefficient of the medium for photons of energy *E*.

The mean free path length $\langle s \rangle$ of the photon until interaction, after it enters the surface of infinite medium can be calculated with the following expression:

$$\langle s \rangle = \int_0^\infty ds\, s\, p(s) = \mu(E) \int_0^\infty ds\, s\, e^{-\mu(E)s} = \frac{1}{\mu(E)}$$

The number of mean free path length *s* is given by:

$$\varepsilon = \frac{s}{\langle s \rangle} = \mu(E)s$$

Defining the number of mean free path lengths as:

$$\varepsilon = \sum_{start}^{p} \mu_i(E)s_i \tag{1.23}$$

Allows expression for the attenuation law that take into account medium heterogeneous to be derived:

$$p(\varepsilon)d\varepsilon = e^{-\varepsilon}d\varepsilon \tag{1.24}$$

The probability weight distribution function $p(\varepsilon)$ is provided by the attenuation law. The cumulative distribution function is given by:

$$P(\varepsilon) = \int_0^\varepsilon d\varepsilon'\, p(\varepsilon') = \int_0^\varepsilon d\varepsilon' e^{-\varepsilon'} = 1 - e^{-\varepsilon} \tag{1.25}$$

The photon is traced on a straight line from its start position on the surface through different regions *i*, containing different materials with linear attenuation coefficients μ_i until the interaction point *P*. In each region *i*, its corresponding line segment s_i must be determined.

The distance to the first interaction site now can be sampled:

$$R_1 = 1 - e^{-\varepsilon_1} \qquad \rightarrow \qquad \varepsilon_1 = -\ln(1 - R_1)$$

where R_1 is randomly generated number in the interval [0:1).

After the photon is moved to the interaction point the type of interaction must be sampled. A random number is sampled in the interval [0, 1] and depending on interval (from p_i to p_{i+1}) its value falls in to, type of interaction is chosen.

photoelectric absorption : $[p_0:p_1)$

raleigh scatter : $[p_1:p_2)$

compton scatter :$[p_2:p_3)$

pair production :$[p_3:p_4]$.

The total interaction cross section is given by the sum of all possible interaction cross sections:

$$\sigma_{tot} = \sigma_A + \sigma_R + \sigma_C + \sigma_P$$

where: σ_A - cross section for photon absorption;

σ_R - cross section for raleigh scatter;

σ_C - cross section for compton scatter;

σ_p - cross section for pair production.

$$p_0 = 0; \quad p_1 = \frac{\sigma_A}{\sigma_{tot}}; \quad p_2 = p_1 + \frac{\sigma_R}{\sigma_{tot}}; \quad p_3 = p_2 + \frac{\sigma_C}{\sigma_{tot}}; \quad p_4 = 1.$$

Angles at which the photon is scattered and its energy is sampled using the probability distributions given by its corresponding differential cross sections. Taking into consideration energy and kinematics conservation laws, all parameters of all secondary particles are determined. The transport simulation of a particle stops when its energy is below predetermined energy cut-off or leaves the geometry. The geometry is represented by a 3D cartesian array of voxels. The way the histories of secondary particles are simulated is based on the same principles. The simulation of electron interactions can be speeded up by applying cumulative-event theories. Because most electron interactions cause small angular deflections and little energy losses, rather than modeling every discrete electron interaction, individual elastic and inelastic events can be combined into single "virtual" event. The accuracy of the calculation can be improved by raising the number of simulated particle histories and decreasing the size of the voxels, however this would also result in slowing down the calculation.

1.5. Quality assurance in radiotherapy

Quality Assurance (QA) is all those planned and systematic actions necessary to provide adequate confidence that a structure, system or component will satisfy given requirements for quality.

Quality assurance in radiation therapy includes all procedures that insure a consistent and safe fulfillment of the dose prescription to the target volume, with minimal dose to normal tissues, and minimal exposure to personnel and adequate patient monitoring aimed at determining the end result of the treatment. Implementation of a quality assurance program reduces errors and accidents.

Quality control is the regulatory process through which the actual quality performance is measured, compared with existing standards, and the actions necessary to keep or regain conformance with the standard. Quality control is part of the larger quality assurance process.

Quality assurance reduces uncertainties and errors in every part of the radiotherapy process, improving dosimetric and geometric accuracy and the precision of dose delivery, thus raises tumor control probability and reduces complications and recurrence rates. In the case of an error occurrence, quality assurance program increases the probability of its recognition sooner. The quality procedures must be adapted to the particular circumstances, equipment and treatment techniques in use.

1.5.1. Requirements on accuracy in radiotherapy

"Accuracy" is a measure of how close a result is to the 'true value' and precision is a measure of the spread of independent determinations of the result where the latter is generally determined as the standard deviation of the distribution of results. Overall uncertainty can be estimated by combined in quadrature the different uncertainties (random and systematic). Random uncertainties can be estimated by repeated independent observations or measurements and can be expressed as a standard deviation of their distribution. Systematic uncertainties can only be assessed by an analysis of the process under consideration.

The accuracy requirements referring to radiation therapy are grounded on the data from dose response curves for TCP and NTCP. Uncertainties leads to reduction in the TCP or increase in NTCP. Uncertainty of 3%, being considered as one relative standard deviation, on the delivered absorbed dose at the dose specification point, can be taken as the currently recommended accuracy requirement [15]. Furthermore, variations in the dose distribution across the target volume may also influence the steepness of practical dose-effect relationships, and hence alter the outcome of the treatment.

Geometric uncertainties arise for a variety of reasons: errors on the field position, block position, simulation and treatment set-up, patient or organ movement during treatment etc., relative to target volumes or organs at risk and they create the potential for localized overdose or underdose. These uncertainties are taken into account by defining margins around the target volume, so estimation of their effect is difficult. Uncertainty of between 5 and 10 mm at 95% confidence level (2 standard deviations) is recommended. The recommended accuracy for the dose delivery is in the range from 5% to 7%. However special cases require better accuracy, for example if very steep complication curves are involved or smaller geometric tolerances are required.

Because the total accuracy depends on the uncertainties at each step of the radiotherapy process, the value of the uncertainty at every step must be kept within an acceptable tolerance.

Estimation of the uncertainties on the total delivered dose requires analysis of the uncertainties at each of the following steps:

1. Determination of the absorbed dose to a reference point in water.
2. Establishment of other doses relative to this.
3. Treatment planning.
4. Delivery to the patient.

Information on the uncertainties at intermediate levels can be provided by the differences in uncertainties at the different steps. Furthermore each step is divided in to substeps. Before equipment is released to clinical use, commissioning measurements must be done and a detailed QA program must be established, which includes also QA test in the case of change in performance, after repair, update or other significant intervention. The frequencies with which the different tests must be done depend upon the acceptable deviation limits of the equipment and its stability over time. The frequencies of the different tests, and the tests themselves vary from center to center. The tests have to provide the required information as quickly as possible with minimal equipment.

QA program for linac includes frequent symmetry, dose monitor, beam energy and others checks, to assure that the machine characteristics do not deviate significantly from their baseline values acquired at the time of acceptance and commissioning. Quality control program must be implemented, also regarding all the additional equipment required to measure radiation doses and to perform electrical or mechanical measurements that is sufficient.

All dosimetry systems (films, ionization chambers etc.) are subject to regular checks and calibration. For example check of the sensitivity of the combination ion chamber - electrometer can be done with Strontium-90. Thermometers and barometers must be regularly checked. Phantoms are subject to regular checks, as well. Their dimensions, densities etc. must be checked before clinical use. Water is the preferred material for phantoms. If plastic materials are used appropriate corrections must be made. Regularly checks for the damage with time are necessary.

In Table. 1.1 are given some of the tolerance levels regarding medical accelerators quality assurance as recommended by the American Association of Physicists in Medicine [16]. It is recommend that "the measurement system and procedure repeatability be such that two standard deviations for three or more repeated consecutive measurements are less than the tolerance value. Linacs used at Dmitry Rogachev Center tolerances are within these tolerance levels.

Table 1.1. *- The tolerance levels regarding intensity-modulated radiotherapy (IMRT) and also the frequency at which it is recommended to be tested.*

Frequency	Machine-type tolerance	Tolerance levels
Daily	X-ray output constancy (all energies)	3 %
	Laser localization	1.5mm
Monthly	X-ray output constancy Electron output constancy Backup monitor chamber constancy	2 %
	Typical dose rate output constancy	2%
	Photon beam profile constancy	1%
	Gantry/collimator angle indicators (cardinal angles)(digital only)	1.0°
	Laser guard-interlock test	Functional
	Treatment couch position indicators	2 mm/1°
	Jaw position indicators (symmetric)	2 mm
	Jaw position indicators (asymmetric)	1 mm
Annual	X-ray flatness change from baseline X-ray symmetry change from baseline X-ray output calibration	1%
	X-ray output constancy vs gantry angle X-ray off-axis factor constancy vs gantry angle Collimator rotation isocenter Gantry rotation isocenter Couch rotation isocenter	1 mm from baseline

Accepting and commissioning of treatment planning system [3] includes tests of its fundamental performance, understanding of its dose calculation algorithms and comparison between the calculated dose distribution and the one measured in a phantom for variety of reference situations. In such a way limitations of the dose computation algorithm can be explored [17]. After software upgrades the planning system have to undergo appropriate acceptance and commissioning program. The uncertainty due to the treatment planning system has to be kept at clinically acceptable levels. The accuracy (geometric and dosimetric) of the planning system should be compared against an agreed-upon standard. Usually accuracy in the range from ±2mm to ±3 mm is acceptable for geometry and from ±2% to ±3% for doses.

It is crucial to transfer the data from the treatment planning system to the treatment machine without any mistakes. In this process usually the data structure of planning system is translated to that of the treatment machine, often user-defined data translation tables are needed. It must be verified that all the information is correctly transferred. The verification process may include data checksum controls embedded in the transferred files.

The IPEM has issued a report [18] on the issue of quality control in radiotherapy. It includes recommendations on quality control program for treatment planning systems. Table 1.2 is from this report and illustrates some of the tests that the treatment planning system has to undergo and the recommended frequencies of these tests.

QA program for treatment planning must also ensure that there are no errors, because of wrong data input, failure of equipment or software bug, and also that the results are interpreted correctly, for every single patient. Therefore individual plans are also subjected to QA procedures. When the dose is varying in unpredictable way gamma index is used. The gamma index is combination of dose and distance criterion. The gamma criteria was used in this work.

Table 1.2. *- Treatment planning system tolerances*

Frequency	Test	Tolerance
Each use	Input/output devices	1 mm
Monthly	Data set – using checksum	No change
Three-monthly	Processor tests	Pass or fail
	CT transfer	1 mm
	Subset of external beam reference plans	2% or 2 mm
Annually	Complete reference plans	2% or 2 mm
	MU calculation	2%

1.5.2. Gama index

To calculate the gamma value [19], [20]corresponding to any measurement point r_m the difference between the measured dose D_m and the calculated dose D_c at this point has to be determined:

$$\delta(\mathrm{r_m}, \mathrm{r_c}) = \mathrm{D_m} - \mathrm{D_c} \tag{1.26}$$

Then the distance r between the nearest measured dose point, r_m that matches the calculated dose at point r_c:

$$\mathrm{r}(\mathrm{r_m}, \mathrm{r_c}) = |\mathrm{r_m}, \mathrm{r_c}| \tag{1.27}$$

Then γ for the measurement point r_m is calculated as follows:

$$\gamma(\mathrm{r_m}) = \min\{\Gamma(\mathrm{r_m}, \mathrm{r_c})\}\,\forall(\mathrm{r_c}), \tag{1.28}$$

where:

$$\Gamma(\mathrm{r_m}, \mathrm{r_c}) = \sqrt{\frac{\mathrm{r}^{\,2}\,(\mathrm{r_m}, \mathrm{r_c})}{\Delta \mathrm{d_m^2}} + \frac{\delta^2(\mathrm{r_m}, \mathrm{r_c})}{\Delta \mathrm{D_m^2}}},$$

Δd_m – passing criteria for isodose distance, (often $\frac{\delta(\mathrm{r_m},\mathrm{r_c})}{\Delta D_m}$ is referred to as percent dose difference);

ΔD - passing criteria for dose, termed also as distance-to-agreement (DTA).

Will the point passes the criteria depends on the value of γ (r_m):

$\gamma(\mathrm{r_m}) \leq 1$ – passes;

$\gamma(\mathrm{r_m}) > 1$– fails to pass.

The value of gamma has to be calculated for all points of interest. The percent of points that passed the criteria determines the overall results of IMRT QA. However, it is also important by how much a certain point passed or failed. All points and their gamma values can be displayed in an iso-γ distribution. Furthermore, the area outside the tolerance range can be allocated to the patient's anatomy. An important feature of this method is that in the final assessment of the dose distribution quality, the value of $\gamma(r_m)$ can be displayed in an iso-γ distribution. The regions where $\gamma(r_m)$ is greater than but nearly unity will be apparent relative to the regions of more significant disagreement. For example, often used acceptance criterion for plan verification is that at least 90% of points need to pass 3%/3 mm criteria [21].

The angle between the dose axis and the γ vector indicates the parameter mostly influencing the γ value. The γ angle is calculated with the absolute values of distance difference and dose difference thus the angle is always in the range from 0 to π/2. For example, γ angles in the range π/4 and π/2 mean that γ index is mostly dominated by the criteria for isodose distance.

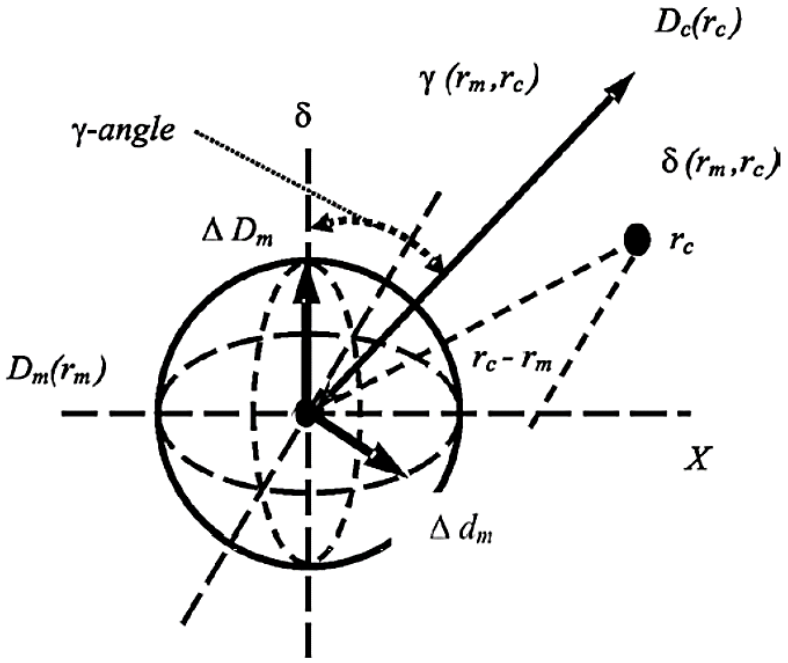

Figure 1.7. *- Definition of the gamma value, $\gamma\ (r_m, r_c)$, and gamma angle*

1.5.3. Clinical Verification of IMRT treatments

Intensity-Modulated Radiotherapy (IMRT) is an extension of conventional Conformal Therapy by purposeful variations or modulations in the intensity across the beam [3]. With IMRT highly uniform coverage of target volumes can be achieved, therefore it allows increased tumor dose with the consequent possibility of an improved cure rate or an improved patient tolerance or both.

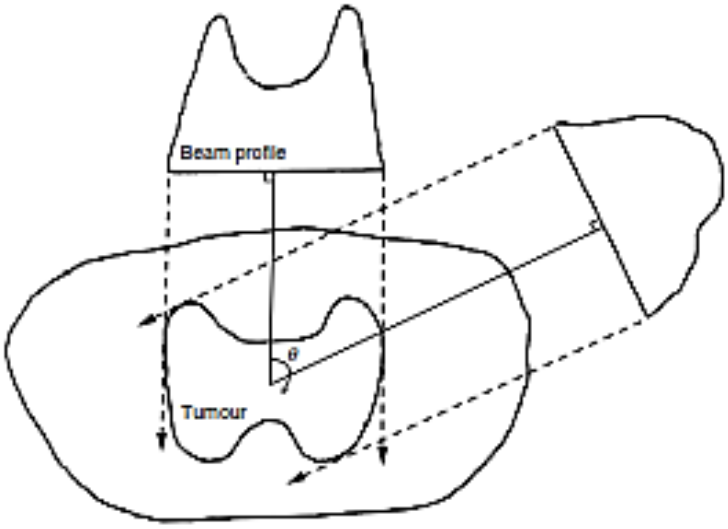

Figure 1.8. *- Concept of intensity-modulated beams. Two of a large set of beams are shown irradiating a 2D slice to achieve conformal dose distribution.*

IMRT involves coordinated motion of the patient couch, gantry, and collimator opening size and shape (of a multileaf collimator). The MLC can efficiently provide irregularly shaped, static, and dynamic, wedged and compensated fields. There is variety of ways to deliver IMRT. Intensity modulated beam can be created by a superposition of open fields with different field shapes. In conventional radiotherapy a set beams with fixed intensity profiles are delivered. The treatment planning computers utilize inverse planning to achieve a pre-defined dose distribution, where some parameters have to be chosen a priori and others are optimized. Intensity-modulation is accomplished by splitting the radiation field in each beam into a large number of beamlets and their optimum weight is determined iteratively. In static IMRT (SMLC or also referred as step and shoot technique) there is MLC motion only during the time-off. The dynamic IMRT (DMLC) involves MLC motion with the beam on. In a Volumetric Modulated Arc Therapy (VMAT) treatment MLC leaves, dose rate and gantry speed are varied concurrently as the gantry rotates around the patient.

To accomplish the desired dose distribution, advanced radiotherapy treatment techniques require a more complex beam delivery system, a MLC with complex leaf motion sequences may be involved, and also the treatment planning process is more complex [20]. For intensity modulation purposes, the radiation field may be created with a number of beams delivered through many small, irregular, and asymmetric MLC, which makes the relationship between the accelerator monitor unit setting and the radiation dose received to the patient more complicated. Oftentimes parameters, which are absent in standard dose calculation are used in IMRT dose calculations. Very much clinical situations can be achieved via IMRT and all of them can't be explored during the model-building process, thus there is higher chance that the

data library, as used by the dose calculation algorithm, will cause discrepancies. Considering the potential consequences of an error, a comprehensive QA should be performed, which includes: commissioning and testing of the treatment planning and delivery systems, routine QA of the delivery system and patient specific dosimetry verification.

Usually individual plans are verified by comparison between the calculated dose distribution and measurement of the actual dose distribution, also the absolute dose must be verified. For these purposes the beam settings are applied to a phantom, then the dose distribution in the phantom is calculated by TPS and next the phantom is irradiated. The phantom dimensions have to be similar to the patient, else the relative contributions of the different beams to the distribution may change. A film or two-dimensional detector array may be situated in the phantom [21].

Then the measured dose distribution can be compared with the calculated in the plane, in which the detector(s) are located. The most common method to analyze the pre-treatment verification is using the Gamma Index Method.

Monte Carlo simulation to verify treatment planning calculations has been investigated [22]. However, more time is needed for computation and it does not provide direct measurement so it doesn't provide additional efficiency to patient specific QA. Measurement-based verification methods can verify the treatment plan, dose calculation in the phantom, plan transfer and delivery. It has been reported that the comparison for IMRT gives systematically lower results (by 1 – 2%) then the results for standard techniques [23], [24].

Korreman [25] used a cylindrical PMMA phantom with two crossing orthogonal planes embedded with 1069 p-Si-diodes for patient-specific VMAT QA. Nine treatment plans were calculated by the treatment planning system and delivered to the phantom. The comparison between the calculated and the measured dose distributions for gamma criteria 3% dose difference and 3 mm DTA demonstrated that more than 95% of points passed the criteria. However, it was pointed out that the interpolation between the two measurement planes to create 3D dose distribution leads to another source of uncertainty [25].

Mans et al. [26] used an electronic portal imaging device (EPID) for VMAT dose verification. EPID's have high resolution in comparison to other QA devices. 3D dose distribution was created via back projection of the frames and application of couch transmission data to all frames separately. To the total 3D dose was applied EPID sensitivity correction. Four patient plans were investigated. The average percentage of points passing gamma criteria 3% maximum dose, 3 mm DTA was 99%. This method has several disadvantages. The algorithm used to include inhomogeneities limits the clinical sites which could be verified. Mans et al. [26] reports also possibility of artifacts at beam-off, beam-on, and changes between discrete dose-

rate levels due to the implementation of the EPID's read-out mechanism, although these effects are averaged out in the final image. Disadvantages of this method also are that EPIDs are highly non-tissue equivalent and many modifications are required before the measured dose distribution can be compared to the calculated.

A hollow cylindrical phantom, embedded with 124 diodes with 2 cm distance between them and forming four rings of detectors, was evaluated by Létourneau et al. [27] for patient-specific QA. The device showed up to 4% gantry angle dependent sensitivity. Correction factors were created for each diode as a function of gantry angle. Comparisons between treatment planning system dose distribution and the measured dose distribution indicated that greater than 86.4% of diodes satisfied a 2 mm DTA and 3% relative dose difference.

Ceberg et al. [28] used a 3D gel measurements for VMAT verification. 3D gel dosimetry advantages are high special resolution, response independent of the gantry and the absorbed dose to an entire volume can be measured. More than 95% passed gamma criteria 3%/3mm. The main disadvantage of this method is that a great deal of manual effort is required for 3D gel dosimetry. The gel used by Ceberg has to be manually prepared 24 hours prior to use and stored in a dark location. To read-out each gel dose matrix has to be scanned on MR or CT. The gel has to reach the equilibrium temperature of the room prior to imaging. The container in which the gel is stored may introduce MR artefacts and inhomogeneities. CT scan of the gel can introduce changes to the gel material, as a result of the absorbed dose during the scan, although this change can be neglected because the dose delivered by the planned treatment is much higher.

1.6. Patient specific quality assurance with MatriXX and its angular dependency

One device designed to perform pre-treatment verification of 2D dose distribution, routine quality assurance of high energy photon and electron beams radiation, for linacs is the MatriXX Evolution, produced by IBA Dosimetry. The MatriXX is a 2-dimensional array of 1020 vented ion chambers, arranged in 32 x 32 grid. The center-to-center distance between chambers is 7.619 mm [29].The MatriXX system comes with a MULTICube phantom and a gantry angle sensor, and it uses OmniPro-I’mRT software. The MatriXX system is described in details at chapter 2.1.

The angular dependence of the MatriXX has been investigated [30], [31], [32], [33], [34], the MatriXX has been reported to over-response up to 6% and under-respond up to 15% [30]. Furthermore, a difference between anterior vs posterior responses up to 11% and large variation of the response as a function of gantry angle in the angle ranges of 91°–110° and 269°–260°was reported[31].

The MatriXX ion chamber array angular dependence has been investigated by Dobler et al. [32].The dose on a CT scan of the MatriXX was calculated for open fields in steps of 10˚. As build-up and scatter material slabs of RW3 were used. At the level of the MatriXX above the iBeam couch an ion chamber was placed and irradiated at 100 MU with a field of 10.4 x 9.6 cm^2 size, at gantry angles for which the doses were calculated. Attenuation due to the couch up to 7% could be observed. In order to take the couch attenuation into account the number of MU was reduced for the respective gantry angle in the treatment planning system calculation, however taking the couch attenuation lead only to slight improvement of the results. Single beam plans were verified and a conclusion that the measured dose was in general higher than calculated for gantry angles in the range 0˚-70˚ and lower for 100˚-180˚ range.

Wolfsberger et al. [31] seventeen IMRT-plans were calculated using collapsed cone, pencil beam, and Monte Carlo algorithms (with the original gantry angles retained) and compared with the MatriXX measured dose distributions. All plans passed the gamma test (> 95% pixels) with 4% dose tolerance and 3 mm DTA. It was concluded that the MatriXX is suitable for hybrid plan verification criteria of 3% and 3 mm with a relaxed dose tolerance of 4% in low dose regions outside the MLC. Off axis correction factors have been found to differ from central detectors correction factors by up to 7%. The doses measured by the MatriXX within specific to the MatriXX phantom were compared to those calculated in a uniform phantom without the MatriXX referred to as reference phantom. The reference phantom geometry closely matched that of the MatriXX phantom. The reference phantom was irradiated with 6 MV beams of 10 x10 cm^2 field size. The dose was measured with an A12 ionization chamber placed along the axis of gantry rotation. The MatriXX within its specific phantom was irradiated with beams of the same energy and field size. Measurements were rendered every 10˚ and at angles in the range 90˚-110˚ and 270˚-260˚ every 1˚. A calibration factor was established at each angle by calculating the ratio of the dose measured with an A12 chamber D_{ref} to the dose measured by the MatriXX D_{mesh} according to eq. (2.2) and (2.3).

Individual „snaps" from the MatriXX record the dose per unit time. They were exported and read by in-house software which applies the calibration factor based on the angle of the recorded snap. The corrected dose distributions were summed and compared to the cumulative dose calculated by the treatment planning system. The same comparisons were made without angular dependency correction. Correction of MatriXX doses improved the agreement between measured and TPS calculated doses. A dose bias of approximately 3% was observed for uncorrected dose distributions, as a result of correction bettered to within about 0.7% with larger discrepancies at the field edges. The comparison also showed that the uncorrected dose distributions and the cumulative dose calculated by the treatment planning system showed a similar

dose distribution shape, however magnitudes of measured dose were consistently smaller. Plans with higher dose gradients demonstrated greater improvement. It was pointed out that the calibration factors are asymmetric, but for the purpose of QA symmetric profile can be derived.

Wolfsberger et al. [31] verified that MatriXX water equivalent build-up and scatter met manufacturer specification and investigated the impact of high-Z material within the MatriXX to AP/PA dose discrepancies. Wolfsberger et al. [31] conclusion was that the angular response of the MatriXX doesn‘t depend on attenuation from the used phantom and cannot be assigned to uncertainties in the density of the MatriXX components or by the uncertainty in Hounsfield units in the planning CT. This difference was attributed primarily to effects occurring at the air-high–Z material interfaces. Furthermore, for lateral beams the effective path length has significant contribution.

Boggula et al. [33] investigated the angular dependence of all MatriXX detectors and used its suitability for verification of VMAT plans. The dose distribution inside the MatriXX inserted in a MULTICube phantom was calculated for a 6 MV beam of field size 28×28 cm^2 from 88 gantry angles in the range from 0˚- 360˚ using Monte Carlo simulation. The MatriXX was irradiated as in the aforementioned treatment plan. To prevent irradiation through the treatment couch the MatriXX was set up vertically. The detector response was acquired using OmniPro-I’mRT software. One of the ion chambers had deviations up to 17 %.The correction factor profiles were asymmetric. To confirm the accuracy of the correction factors 12 VMAT plans were investigated by gamma criterion. When the criterion was 2% dose difference and distance to agreement 2mm the minimum, maximum and mean percentages of passing points were as follows. Before angular correction - 77.0%, 99.5% and (89.0 ± 7.0)%, respectively and after the correction were 83.5%, 99.5% and (93.2 ± 4.6)%, respectively. When the criterion was 3% dose difference and distance to agreement 3mm the minimum, maximum and mean percentages of passing points before the correction were 94.6%, 100.0% and (98.6 ± 1.9)%, respectively. After the correction they were 95.3%, 100.0% and (99.0 ± 1.6)% respectively.

Shimohigasi at el. [30] measured and calculated by Monte Carlo algorithm the MatriXX dose distributions, when placed inside the MULTICube phantom for 27 gantry angles in the range 0˚-180˚. Field size of 30 x 10cm^2 for 6 MV and 10 MV photons were chosen. The MatriXX was placed vertically to avoid couch attenuation. Two sets of angular correction factors were created for each of the beam energies. The first was derived from the average dose of four detectors at the center of the MatriXX array. For the second set individual correction factor was derived for the off-axis columns (column corresponds to the X axis), which were based on the average dose of the two detectors at rows 16, 17. It was assumed that the correction factors for gantry angles in the range 180˚- 360˚ are the same as the correction factors for gantry angles of

0°–180°.The difference between the central correction and off-axis correction factors were calculated by the ratio of the subtracted central correction factor from the column correction factor to the central correction factor. Furthermore, the correction factors were validated with different fields, Monte Carlo calculated treatment plans including IMRT and VMAT plans and film (ISP-RTQA2) measurements. Absolute doses measured with the MatriXX were compared with ionization chamber (PTW-TN31010 Semiflex 0.125 cc thimble chamber). Before the correction MatriXX doses deviated by up to -7% and -6% from the chamber measured doses for 6 MV and 10 MV, respectively. After the correction the dose deviation was within 2%. The MatriXX detectors demonstrated under-responses of up to 15% and 11% at 92° and over-responses of up to 6% and 4% at 90° for 6 MV and 10 MV photons, respectively. The treatment plans and their corresponding MatriXX measurements were compared by gamma criterion. When 2% dose difference, distance to agreement 2mm and 5% threshold were chosen at gantry angle 90° results for "no correction," "central correction," and "entire correction" were the following: for 6 MV photons 81%, 79%, and 93%, respectively; for 10 MV photons 86%, 85%, and 95%, respectively. The improvement of passing rate increased for off-axis correction with the increasing of field size. It was also reported that a dose bias up to 5.1% was observed for dose verifications of IMRT plans, which was reduced to within 2% after angular correction was applied. It was stated that the differences in an improvement of the passing rates is not the same as et al [33] for VMAT QA, due to a difference in the number of arcs.

EBT films have also been used successfully as a reference dosimeter, to determine the angular correction factors [34].

When a single correction factor is applied to all chambers, usually it is derived from the average signal of the 4 chambers situated at the center of the chamber array. Several issues when using a single correction facture were pointed out when along with the MatriXX a rectangular phantom is used [33].The beam gets harder at the center detectors away from perpendicular incidences. At angles 0˚ and 180˚ the beam has to pass minimum build-up to reach the central chambers and at angles 45˚, 135˚, 225˚, 315˚, it passes maximum build-up. However, this is not the case for all other chambers, thus the energy spectrum for different chambers is not the same. The effective angle is different for chambers located at different positions on the X axis. Due to this effects improper calibration factor will be applied to some of the detectors. It was also noted that in order to reduce uncertainty due to couch attenuation (for carbon couches the attenuation varies between 2% and 10%) the couch top used in the treatment room should be identical to the couch top used for patient imaging.

Discrepancies between the calculated and measured dose distributions were explicitly seen at the field edges. This was attributed to variety of factors: uncertainties in the collimator

position (about 1mm), leaf position reproducibility, slight positional errors and uncertainties of the chambers measurements, MatriXX resolution. Other issues are the monitor output fluctuation of treatment machine [35], dose stability during gantry rotation and accuracy of gantry angle. The measured doses at a single point in modulated beams could vary up to 13% under specific circumstances [36]. When a beam is highly modulated between detectors the measured and the calculated doses may differ significantly**.**

Uncertainties associated with the Monte Carlo simulation also contribute to the difference between calculations a measurements. The computation of dose under the collimators may not be accurate, because it depends on the linac head simulation. Generally it is less accurate out of the active beam area.

2. Experimental part

2.1. Equipment

In order to correct the angular dependency distributions, it is necessary to derive reference dose distributions. The reference distributions should be as close as possible to the actual dose distributions within the MatriXX. Reference distributions were obtained with EBT2 films and the Monaco Monte Carlo algorithm.

2.1.1. MatriXX Evolution system

The MatriXX Evolution is a 2-dimensional array of 1020 vented ion chambers, arranged in 32 x 32 grid. The center-to-center distance between chambers is 7.619 mm [29].The chamber current is measured and digitalized by a non-multiplexed 1020 channels current sensitive analog to digital converter.

Figure 2.1. *- MatriXX Evloution*

The MatriXX Evolution provides a measurement of absolute dose in each ion chamber ($D_{i,j}$). A calibration of the gain for individual ion chambers is given by the manufacturer [29] and the absolute calibration of the detector response has to be done by the user. The conversion from charge measured by the MatriXX electrometer to absolute dose $D_{i,j}$ in the effective measurement point for each individual chamber at location i, j is described by equation:

$$D_{i,j} = (M - B)_{i,j} N_{DM}^{^{60}Co} K_{uni\,ij} K_{off\,i,j} K_{User} K_{pT} \qquad (2.1)$$

where $M_{i,j}$ is the raw measured signal, $B_{i,j}$ is the signal due to background, ($N_{DM}^{^{60}Co} K_{uni\,ij}$) is the Uniformity Correction Matrix, i.e. the uniformity calibration matrix, multiplied with calibration to cobalt in Gy/nC at reference temperature and pressure, $K_{off\,i,j}$ is the off-axis calibration factor (determined by the user), $K_{T,P}$ is correction for temperature and pressure, and K_{user} is the user calibration factor for the detector.

The $N_{DM}^{^{60}Co} K_{uni\,ij}$ factor is measured and calculated at the production site. $(M - B)_{i,j}$ and K_{pT} are measured and calculated by the MatriXX system. The $K_{off\,i,j}$ and K_{user} factors can be created by the user. $K_{off\,i,j}$ is a user-defined calibration factor which compensates for deviations that occur after the MatriXX has been in use for some time. The K_{user} is created by the user, for its determination the MatriXX Evolution is irradiated with known dose at the effective point of the ion chamber, while in the MULTICube phantom with a 10 × 10 cm^2 field. In table 2.1 are listed some of the MatriXX specifications.

Table 2.1. - MatriXX specifications

Warm-up time	15 – 60 min
Chamber diameter	4.5 mm
Chamber height	5 mm
Chamber volume	0,08 ccm
Distance between chambers	7,619 mm
Nominal sensitivity	2.4 nC/Gy
Maximum dose rate	20 Gy/min
Minimum dose rate	0.02 Gy/min
Bias voltage	500 ±30 V
effective point of measurement	3,5 mm
Absorber material on top	ABS (density 1,06)
Water equivalent depth	3,2 ± 0,5 mm
Minimum sampling period	20 ms
Non-linearity	± 0.5%
Data link	0/100 baseT
Communication protocol	TCP/IP
Mains voltage range	100 V to 240 V AC ±10 %
Max. power consumption	15 W

The MatriXX uses OmniPro I'mRT software. OmniPro I'mRT system is designed for treatment plan verification and quality control. Data can be imported in the OmniPro I'mRT from the treatment planning system and electronic devices such as MatrixXX [29]. OmniPro I'mRT software performs comparisons between dose or fluence distribution calculated by the treatment planning system and a measured distribution. For example it can compare absolute dose in single points, intensity maps and relative doses [29].

The Plastic Water phantom MULTICube *Lite* is used together with MatriXX Evolution for Rotational Dosimetry application. Plastic Water have mass density 1.030 g/cm^3 and electron density 3.337 × 10^{23} g/cm^3. The Plastic Water phantom outer dimensions are (L × w ×h) 34 cm × 31.4 cm × 21.9 cm and weigh 19.8 kg [37]. The manufacturer provides film cassette consisting of 3 components (top, bottom and cover plate) with total thickness 3.9 cm for film measurements.

Figure 2.2. *- Setup of the MatriXX Evolution within MULTICube Lite*

A possible warm-up behavior the MatriXX and the consistency of ion chamber responses were investigated.

Included in the MatriXX system is a gantry angle sensor used for online detection of the gantry angle during irradiation, when affixed to the gantry. The accuracy of the angle sensor is ±0.5°.

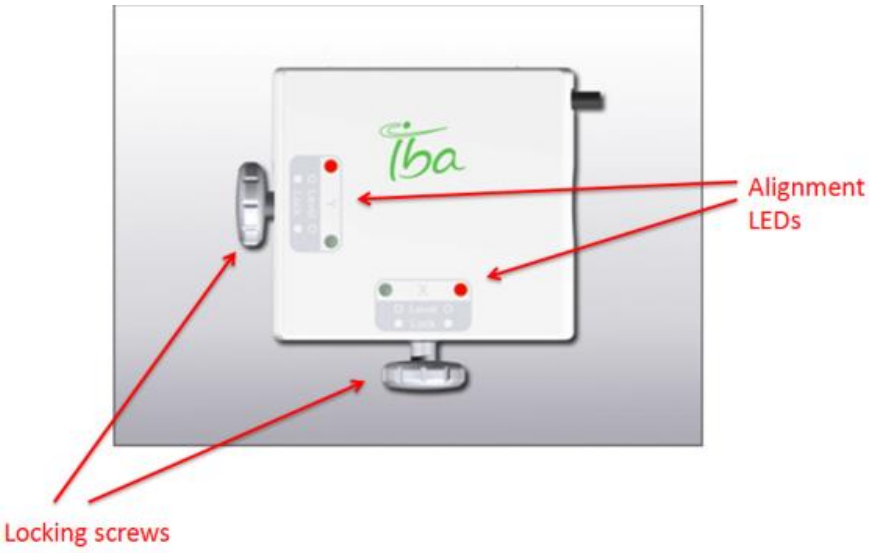

Figure 2.3. *- Gantry angle sensor*

The MatriXX can be used for the measurement of radiation beams with oblique angles of incidence; however angular dependence of the ion chambers is present, which causes small discrepancies when comparing MatriXX measured dose distributions to the computed reference doses. The angular dependence is due to the internal structure of the MatriXX device. The angular dependency of the ion chambers can be taken into account by multiplication of the measured signal from each individual chamber and a gantry angle dependent correction factor [29]. The gantry angle is measured by the gantry angle sensor. Correction factors $C_{i,j}(\theta)$ of the MatriXX detector at row *i* and column *j* at gantry angle θ are calculated from the ratio of the MatriXX-measured dose to reference doses at that angle .$C_{i,j}$ is defined as:

$$C_{i,j}(\theta) = N_{i,j}\frac{D_{i,j}^{ref}(\theta)}{D_{i,j}^{meas}(\theta)} \tag{2.2}$$

where $N_{i,j}$ is factor that normalizes $C_{i,j}$, such that:

$$C_{i,j}(0^{\circ}) = 1. \tag{2.3}$$

The sets of correction factors are stored in "comma separated value" (csv) files (named also look up table or LUT), along with the angle at which they should be applied [29]. Detailed information about the file is given in Appendix A.2.

The software linearly interpolates between the correction factors of the angles to create factors of angles which are not present in the LUT and also linearly interpolates the correction factors between qualities to create a customized correction factors for the data.

The manufacturer provided correction factors for 6MV and 18MV photon beams, which are valid for the combination of MatriXX Evolution with MULTICube *Lite*. For those angular correction factors it is assumed that all chambers of the MatriXX array exhibit the same angular dependence and symmetry between the angles which range from $0^{\circ} - 180^{\circ}$ and $180^{\circ} - 360^{\circ}$ which results in $C_{i,j}(\theta) = C_{i,j}(360^{\circ} - \theta)$. The manufacturer LUT consists of correction factors for angles between 0˚ and 360˚with an angular resolution of 5˚ except in the ranges from 85˚to 95˚ and from 265˚ to 275˚ where an angular resolution of 1˚ was used. Appling the manufacturer LUT to measured dose distributions slightly (less than 1%) improves the results of comparisons between measured and treatment planning system calculated dose distributions.

In this study custom sets of correction factor tables were created and imported into the OmniPro-I'm*RT*software. The custom correction factors take into account the specifics of the MatriXX, phantom, accelerator and couch used at the Federal Research and Clinical Center of Pediatric Hematology, Oncology and Immunology "Dmitry Rogachev".

2.1.2. Gafchromic EBT2 films

With EBT2 dosimetry dose errors within 1% can be achieved [38], which makes it suitable for measurement of reference dose distributions used for creation of MatriXX angular dependent correction factors.

Gafchromic EBT2 film has a multilayer structure made by combining a clear, polyester over-laminate with the active film coating [39]. The substrate of the active film is clear polyester (175μm thickness) coated with an active layer film (nominally 30 μm thickness). Over the active layer there is a topcoat, nominally 5 μm. Bonded to the coated side of the active film is an over-laminate of 50 μm polyester with approximately 25 μm of pressure-sensitive adhesive. EBT2 has effective atomic number 6.84. The configuration of EBT2 film is shown in Figure 2.4.

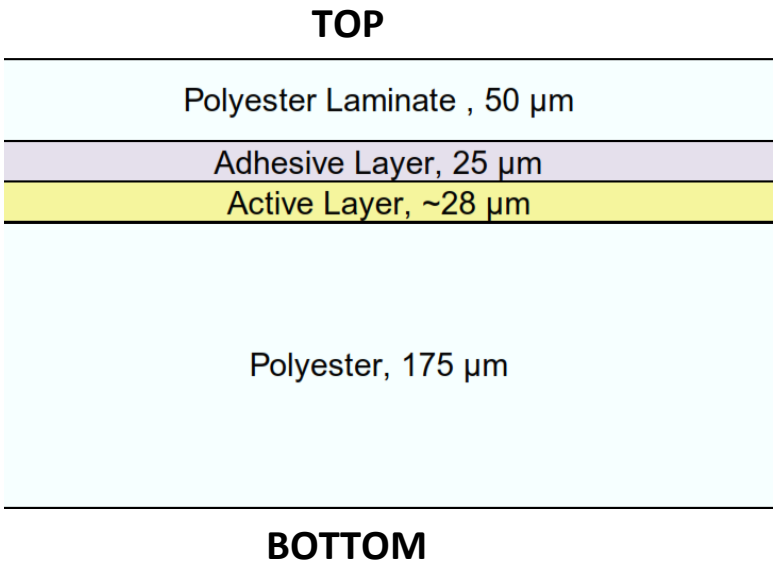

Figure 2.4. *- Structure of EBT2 Gafchromic film*

The bottom surface can be distinguished from the top surface, because bottom surface reflection appears to be blurred compared to fluorescent light reflection from the top surface. The over-laminate protects the layers under it from mechanical damage and water. Dye is incorporated in the active layer, in order to establish a reference against which the film response can be measured. Thus a net film response independent of small differences in the thickness of the active layer can be obtained. Exposure of the active layer to radiation leads to formation of polymer with absorption maxima at about 585 nm and 636 nm.

For the reason that post exposure changes (proportional to the function of time) occur it is necessary to scan or measure all films, including calibration films after the same time has passed since exposure. It is to recommend to scan the films at least 2 hours after exposure (for relative dosimetry post-exposure timing is not essential). After 4 hours the approximate change in dose/min is 0.01%.

2.1.3. Monaco treatment planning system

Monaco is a Monte Carlo-based treatment planning system which is designed to create treatment plans for patients with prescriptions for external beam radiation therapy [40]. The planning system calculates and presents, on-screen and in hard-copy the dose and its distribution inside patients or a phantoms for a given treatment plan set-ups. Dose distributions with user-defined statistical uncertainty can be obtained. Reference dose distributions calculated by Monaco, with statistical uncertainty of 0.6% were used for the creation of correction factor sets. The final Monaco dose calculation is based upon the original Voxel based Monte Carlo, which is modified and renamed to X-ray Voxel Monte Carlo (XVMC) [40]. In preference to detailed MC simulation of the linac head the MC algorithm utilize a Virtual Source Model (VSM) [40], based on measured data to increase the speed of calculation, voxelized patient geometry is used. To create a patient model CT data is converted to relative electron density and the electron density is converted to mass density. Afterwards, the Monte Carlo transport is initiated. From the source model the particle energy, position, and angle of trajectory are determined by analytic functions.

The virtual source model consist of a primary photon source, scatter photon source, and electron contamination source [40]. To create the VSM first various in-water measurements have to be acquired, then based on measurements the individual sources are described with the most appropriate analytic functions. Analytical method named transmission filter is used to model the flattening filter, primary collimator, jaws and MLC. During modeling are determined the source position, size and weight, also the energy spectra both off and on axis. Based on the weights of the virtual sources random number generator generates the particle.

First the type of particle is chosen. Then is determined the initial position of the particle, proceeding from sampling the particle energy and source size. Afterwards, is calculated the probability of traversing through the flattening filter, MLC leaves and jaws is determined using the transmission filter model. The particles in the patient are tracked by XVMC Monte Carlo method, with cut-off energies for photons 50 keV and for electrons 500 keV. The patient model in which dose is calculated is generated from a patient CT study set. A dose grid made up of cubic voxels is superimposed upon the CT study set. The voxel size can be selected by the user. Each voxel is subdivided into 27 sub-voxels. At the center of each sub-voxel the electron density is sampled. Then the average electron density from all sub-voxels is assigned as density of the voxel they belong to. Outside the patient contour the electron density is set to zero. The dose voxels extend beyond the patient surface at the patient boundary. The Hounsfield units from the contoured voxelized patient are mapped to relative electron density via scanner specific CT to electron density curve created by the user. Next the electron density is converted to mass

density by theoretical curve. The conversion from HU to mass density has inherent errors, because of the approximation of irregular shapes with voxels and averaging over different density structures. The mass density is calculated accurately in the range 0-3 g/cm. Beyond 3g/cm the accuracy of the calculated dose deposition is degraded, however radiation transmission is accurate. The dose deposited to object with mass density less than 3g/cm immediately adjacent to a high density object is not degraded. For metallic lead (11g/cc) the dose deposition error can be up to 5%. Selecting smaller voxels will improve dose accuracy in regions of high density gradients, and in regions of high dose gradients, however the calculation will take more time.

The interaction probabilities are based on the attenuation coefficients and electron densities from ICRU Report 46 [41]. The methods for sampling energies and scattering described in EGS4 [42] are used. After all interaction values are computed for all voxels the particle tracking begins.

Approximations and simplifications are used to speed up the calculation. The average number of secondary particles generated is based on the number emitted in homogeneous water, instead the ones emitted in the material of interest. The dose calculation uses a continuous density material approximation. After electron history for two monoenergetic beams is generated, the electron history is translated to multiple locations. Systematic bias of about 0.5% is created by the history repetition, this is one of the main reasons why the model is more accurate for low Z material and energies below 25 MeV. Inherent statistical uncertainty of 0.5% is not significant compared to the typical statistical uncertainty inherent in Monte Carlo calculations.

In Monaco the user selects the statistical uncertainty. The number of particles generated by the source model is determined at the beginning of the calculation based upon an empiric equation.

2.2. Accelerator calibration

Prior to MatriXX measurements both identical Synergy and Synergy Platform accelerators provided with Agility MLC and used at Clinical Center “Dmitry Rogachev” were calibrated, as recommended by the International Atomic Energy Agency in the Technical Reports Series No 398(TRS-398) [9]. Cylindrical ionization chambers FC-65-G Farmer type was used. The temperature and pressure were measured and the correction factor for the changes in the air mass within the cavity was calculated by eq. (1.16), a correction factor for the for polarity effect p_{pol} was calculated according to eq. (1.20). After that the beam quality index Q was evaluated. The beam quality for high-energy photons used in radiotherapy is specified by the tissue-phantom ratio $TPR_{20,10}$.

$TPR_{20,10}$ is defined as the ratio of the absorbed doses at depths of 20 cm and 10 cm in a water phantom, measured with a constant source-chamber distance, SCD of 100 cm and a field size of 10cm x 10 cm at the plane of the chamber[9]. $TPR_{20,10}$ is not influenced by electron contamination in the incident beam. It describes the decrease of a photon depth-dose curve beyond the depth of maximum dose.

When cylindrical chamber is used for its measurement, displacement correction factors are not needed. $TPR_{20,10}$ is not affected by small systematic errors in positioning the chamber in most clinical set ups, because the settings at both positions will be affected.

The chamber was under irradiated at conditions according with the reference conditions given in TRS-398 (SCD = 100 cm at depths 10 cm and 20 cm, field size 10cm x 10cm). It was placed in a water phantom as shown on fig.2.5. The influence of recombination effects at the two depths was investigated and taken into account according to formula (1.19) where the values of a_i were taken from TRS-398 [9].

The ionization chamber was positioned in reference conditions (SCD = 100 cm at depth 10 cm in a water phantom, field size 10cm x 10cm). The absorbed dose to water, in a beam of quality Q in these reference conditions, at the position of the reference point of the chamber is given by the following expression:

$$D_{w,Q} = M_Q N_{w,D,Q_0} k_{Q,Q_0} \qquad (2.4)$$

where M_Q is the reading of the chamber corrected for the influence of temperature, pressure, electrometer calibration, polarity effect and ion recombination. $N_{w,D,Qo}$ is the calibration factor in terms absorbed dose to water for the chamber at reference quality Q_o, and $k_{Q,Qo}$ is a specific factor for the chamber, which corrects for the difference between the actual quality Q and the reference beam quality Q_0. The value of k_{QQo} for the chamber presented in TRS-398[9] was used.

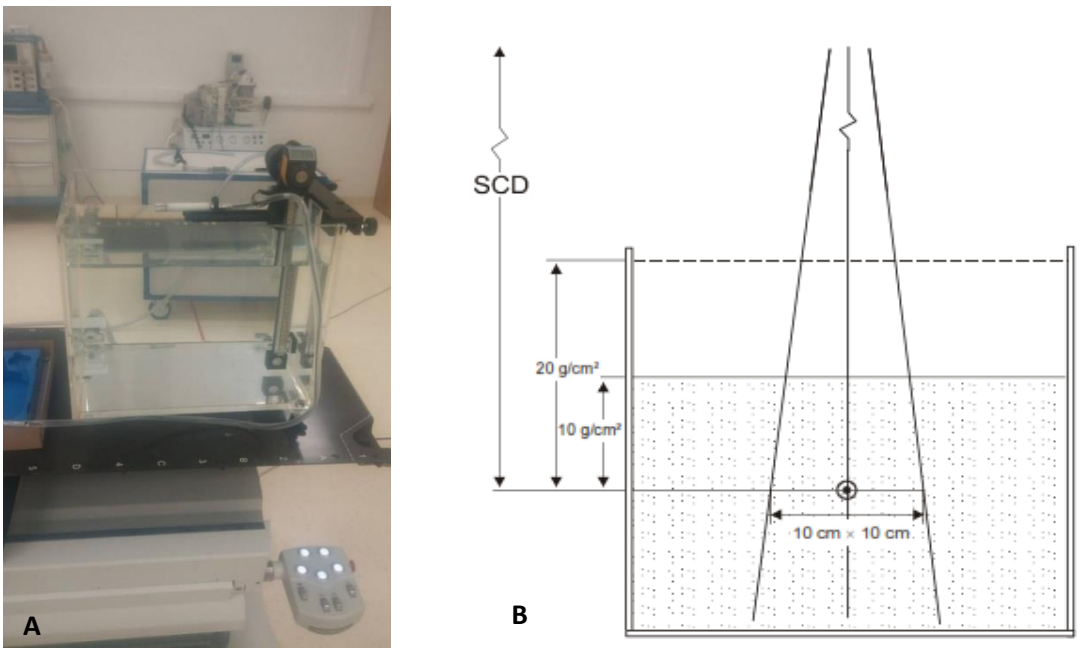

Figure 2.5 *- Experimental set-up for the determination of the $TPR_{10,20}$.* ***A.*** *Water phantom and Farmar chamber.* ***B****. Scheme of the set-up. The SCD is kept 100 cm and measurements are made with 20 g cm^{-2} and 10 g cm^{-2} of water over the chamber. The field size at the position of the reference point of the chamber is 10 cm x 10 cm.*

2.3. Tests of the equipment

2.3.1. MatriXX warm-up

To analyze a possible warm-up behavior the MatriXX was placed within the MU'LTICube phantom and irradiated 3 times with 6MV x-rays 100 MU and a field size of 20 x 20 cm^2 without and with a warm-up period. The time interval between irradiations was 5 min and the warm-up period was, as recommended by the manufacturer 1 hour

Table 2.2 shows the results of the MatriXX irradiation with and without warm-up period. There is an increase of the signal with every measurement (every 5 min) of nearly 0.01%. After warm-up of 1 hour the change of the signal of the detector is not detectable. The uncertainty of the measured dose is higher than its actual value, as a result of dose variations over the target. Using the MatriXX without being warmed-up would lead to underestimation of the dose of about 0.04% percent.

Table 2.2. - *MatriXX warm-up*

Measurement	D,Gy(without warm-up)	ΔD,Gy	D,Gy(warmed-up)	ΔD,Gy
1	1.014	0.014	1.018	0.014
2	1.015	0.014	1.018	0.014
3	1.016	0.014	1.018	0.014

2.3.2. MatriXX individual ion chambers response consistency

To evaluate the consistency the MatriXX chamber responses the MatriXX was irradiated with 100 MU, 6MV beam of size 30 x 40 cm^2 at gantry angles 0˚, 45˚, 90˚, 120˚ and 180˚. Five measurements were obtained at each angle. The standard deviation was calculated for each chamber for every angle. The average standard deviation was in the range 1.1% - 0.73%.The average standard deviation between all ion chamber over all angles was 0.82%.The consistency of the chambers responses were not significantly affected by the gantry angle. At angle 0˚ the standard deviation from the mean value of all detectors responses was 1.11%. However that value is overestimated, as a consequence of dose variations in the transverse plane. The difference in response between chambers at angle 0˚ is not substantial, considering that the mean uncertainty in response of each ion chamber was 0.82% at this angle. Therefore, correction factors at angle 0˚would be inefficient.

2.3.3. Radiation output intensity fluctuations at different gantry angles

To evaluate X-ray output constancy as a function of the gantry, MatriXX detector was mounted on the gantry using an Elektra holder and connected with OmniPro IMRT verification software. The holder of MatriXX consists of a XY table and a supporting frame. The supporting frame holds the MatriXX and build-up plates. The source-to-detector distance in the gantry mount was 100 cm. Backscatter plates made of water equivalent polystyrene, RW3 can be mounted from 10 to 100 mm, in steps of 1, 2, 5 and 10 mm on the top and bottom of the detector. On top of the MatriXX. 4 cm of polystyrene build-up was placed. Preirradiation of 500 MU was given to the MatriXX. A 20 × 20 cm^2 6MV x-ray field, 100 MU was delivered to the MatriXX. The field was delivered for gantry angles from 0° to 350° in 10° increments, starting from 180° in clockwise direction. The experiment was conducted a second time, but the field was delivered starting from 180° in anticlockwise direction. The same experiment was repeated for second linac.

Figure 2.6 shows how the delivered dose at the different angles normalized to the delivered dose at angle 0˚ vary with the angle.

There is no significant change in the delivered dose as the gantry rotates (no more than 0.8%), given the fact that X-ray output constancy recommended by the American Association of Physicists in Medicine tolerance level is 3% (see table 1.1). The change of the delivered dose at different gantry angles can be neglected in the calculation of correction factors.

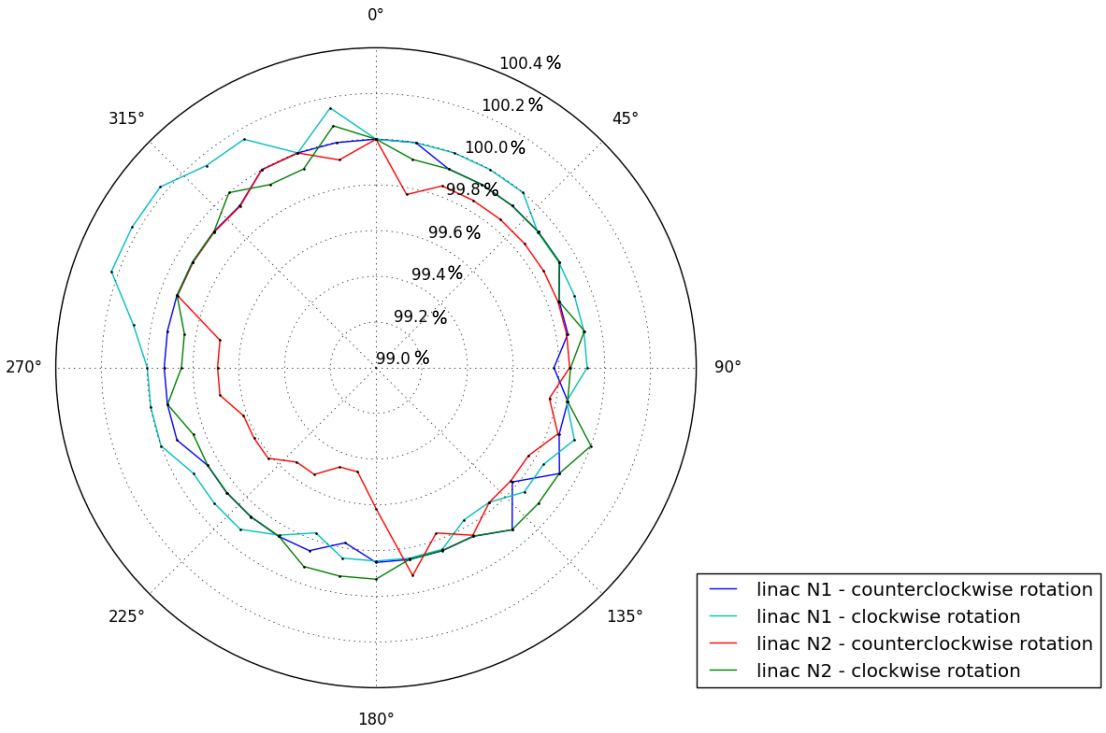

Figure 2.6. *- Gantry angle delivered dose dependence. The average of the read of the detectors situated in square with a side 14 cm, was used as the result. Difference between the maximum and minimum delivered doses is less than 1%.*

2.4. Creation of angle dependent correction Factor sets

In order to correct for the inherent gantry angle dependence, 32 x 32 matrixes of correction factors were created by taking the ratio of measured dose to reference dose and normalizing them to gantry angle 0˚. Correction factors were created for 6, 10 and 15 MV using a subset of gantry angles.

Measurements were acquired using MatriXX Evoluton for static open fields delivered at gantry angles from 0˚ to 360˚.The delivered to the MatriXX doses at this angles were also calculated using Monaco treatment planning system. Furthermore, film measurements were acquired for the angles in the range 0˚-180˚ to be used for the derivation of another set of factors for 6MV photons.

2.4.1. MatriXX measurements

Measurements with the MatriXX were conducted with the ion chamber array placed within MULTICube phantom. The MatriXX was positioned at the linac isocenter on the i-BeamEVO treatment couch with the assistance of laser alignments. The MatriXX was positioned such that the detector plane faced gantry angle 0°. The initial setup is shown in Figure 2.7.

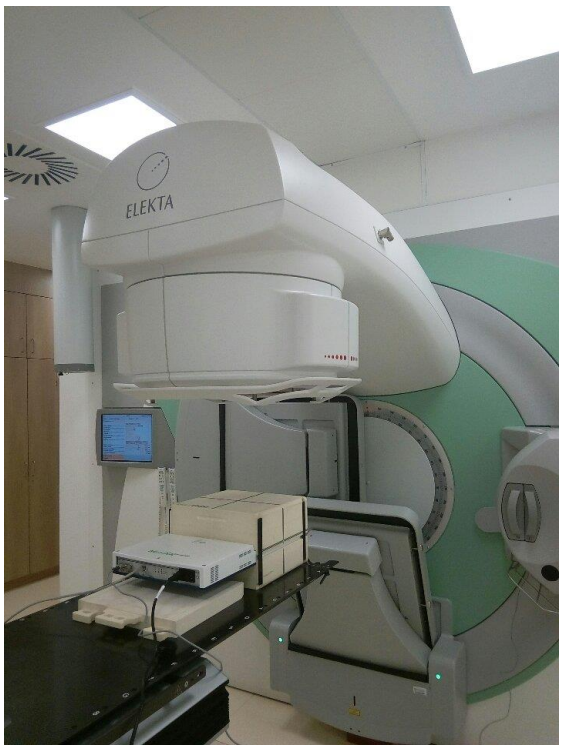

Figure 2.7. *- The MatriXX placed on the couch at the linac isocenter.*

Measurements were acquired on two identical Synergy accelerators which utilize identical couches. The gantry angle sensor was attached to the gantry, its correct alignment was indicated by LEDs. The angle sensor was calibrated at gantry angles 0° and 90° by the OmniPro software. The MatriXX was warmed-up for 1 hour and pre-irradiated prior to use, until the detectors signals reach a stable value. The pre-irradiation open field was delivered at gantry angle 0˚ and the MatriXX was in face up position. The MatriXX was connected to a power source, gantry angle sensor, and PC. Measurements were processed by OmniPro I'mRT v.1.7 software. The background signal (without any beam incident on the MatriXX) was collected in order to be automatically removed from subsequent measurements. The MatriXX was irradiated with 100 MU and field size 30 x 40 cm^2. The measurements were acquired in 5° increments for angles in the range from 0˚ to 360°, except for angles 85° to 95° and 265° to 275° where increment was 1°. The dose delivered to the MatriXX was recorded by the OmniPro I'mRT software in "movie mode", where during delivery individual "snaps" are obtained every 500 ms and summed to create an "integral" dose. The measured dose distributions from both lines were compared for the-same angles and found to differ up to 1.6 %, however for most angles the difference was less than 1%. Dose distributions from both linacs for each irradiated angle were summed and the summed dose exported from OmniPro I'mRT in ASCII format and read into Python3, where they were divided by 2 to obtain the average dose. Within Python, several different ways were used to create LUTs.

2.4.2. Reference dose distributions via Monte Carlo calculation

CT scan of the MatriXX was imported in the Monaco system. The electron densities specified by the manufacturer were given to the absorber material on top of the MariXX and MULTICube, to avoid possible small inherent errors from the Monaco conversion of HU to mass density. Model of the used couch was given by the manufacturer, which allowed for TPS calculation of the MatriXX dose when the MatriXX is placed on the couch. So the effect of couch attenuation is implicitly taken into account.

The Monaco Monte Carlo algorithm was used to calculate expected doses to the MatriXX at every gantry angle and energy the MatriXX was irradiated. The doses were calculated for the same condition used for MatriXX irradiation (100 MU, 30x40cm^2 field size, MatriXX placed within the MULTICube on the couch at the isocenter). The dose calculation was performed at uncertainty of 0.6% and 0.2 mm grid size.

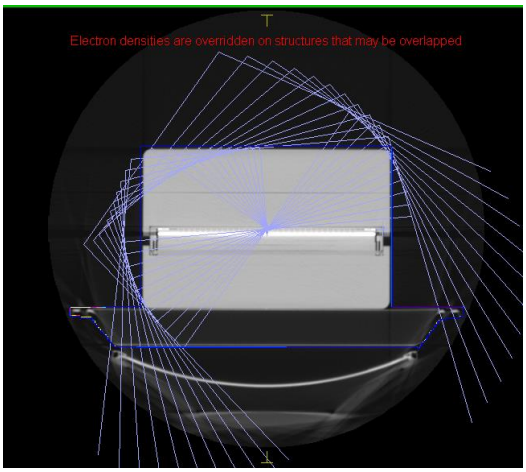

Figure 2.8. *- Image of the MatriXX as it is shown in the TPS. This plan calculated the expected doses to the MatriXX at gantry angles 305˚ – 355˚.*

The dose distributions were exported from Monaco for each of the gantry angles in DICOM format and imported into the OmniPro I'mRT software. The doses calculated by Monaco were used as reference for creating the correction factors.

2.4.3. Measurements of reference doses via film

To determine the dose after exposure with film measurement, calibration of the film scanner is necessary. EBT2 film sensitivity is dependent upon parameters like batch, age, type or storage conditions. For this reason it is necessary to perform calibration specific to the batch from which the films belong. It is possible to perform a direct scanner signal to dose calibration.

Calibration curve was obtained by irradiating films with known absorbed doses, then scanning them with Microtek 9800 scanner and obtaining the values from the analog to digital

converter. The system was calibrated for beam energy 6MV. To determine the connection between 1MU and the dose delivered to the film in the particular geometry of measurement, FC-65-G Farmer type ionization chamber was irradiated in the same conditions as the films will be irradiated in. Irradiations were performed with field size 30x30 cm^2 at 100 cm SAD. 100 MU were delivered to the ion chamber and its reading was corrected for the beam quality of 6MV beam. The dose delivered to the chamber was divided by the number of MU to establish a coefficient with unit Gy/MU. A film was cut into a set of pieces of size 5x20cm^2 and pre-scanned 5 times to correct for intensity variations in the scanner light, then irradiated to dose levels of 0.4, 0.7, 0.9, 1.1, 1.5, 1.8, 2, 3.5, 5 Gy and one piece was not irradiated. Each film piece was placed on top of a solid water build-up with thickness 10 cm and 10 cm build was placed on top of the film piece (the same build up was used for the ion chamber).Irradiations were performed with field size 30x30 cm^2 at 100 cm SAD and 100 MU.

Prior to scanning the film pieces 5 empty scans were done to warm-up the scanner. Four hours after irradiation all film pieces were positioned at the center of the scan field and scanned five times. This calibration method was applied to web software, placed at www.radiochromic.com. The 5 scans prior to irradiation were merged together in order to obtain a single scan with less noise. The 5 scans after irradiation were merged into a single scan and the values from the analog-to digital converter (ADC) were obtained selecting the center section as region of interest (ROI) with a cursor. The user enters the corresponding doses to the ADC values and the software creates the calibration curve. To determine unknown dose after exposure with film measurement, the user has to apply the calibration to the film scan. Furthermore the user can chose ROI over which the average dose will be calculated.

Films from the batch used for calibration were taken and cut into 45 pieces of size 3.8 x 5.08 cm^2. The film pieces were irradiated with 6 MV photon beam of 30 x 40 cm^2 and 100 MU at gantry angles from 0˚ to 180˚ in steps of 5˚, in the range 85˚ to 95˚ where film measurements in steps of 1˚ were obtained. A film piece was positioned within the MULTICube phantom inside specific to the MULTICube film insert at the same position as the central MatriXX ionization chambers. The film pieces were positioned at the center of the scan field in the same orientation as the film pieces used for calibration and scanned 3 times 4 hours after irradiation. The scans were imported in www.radiochromic.com, the aforementioned calibration was applied in order to obtain the film doses. ROI corresponding to the 4 central detectors was chosen and the average dose over that ROI acquired and recorded into Excel table. Further these doses were used to create custom LUTs.

2.4.4. Analysis of the measured and calculated doses symmetry using two-sample Kolmogorov–Smirnoff test

To test whether the MatriXX measured doses differ from each other for gantry angles 0˚-180˚ and 180˚ - 360˚ they can be statistically analyzed using two-sample Kolmogorov–Smirnoff test. To test whether the TPS-calculated doses at various gantry angles differ from each other, the same test can be used. The two-sample Kolmogorov–Smirnoff is non-parametrical test that determines whether the two samples come from identical distributions [44]. For each sample *k* of size S_k empirical distribution is constructed via step function $F_{s_k}(x)$.

$$F_{s_k}(x) = \frac{s}{S_k} \quad \text{when} \quad x_i^{sample\ k} \leq x \leq x_{i+1}^{sample\ k} \tag{2.5}$$

where s is the number of observations equal to or less than *x* and $x_{i+1}^{sample\ k}$ are the order statistics for the sample.

The two empirical distributions are compared by calculation of their maximum absolute difference as:

$$D = max\left|F_{s_1}(x) - F_{s_2}(x)\right| \tag{2.6}$$

The null hypothesis is that the samples are drawn from the same distribution. If the null hypothesis is true the value of *D* should be small. To reject the null hypothesis the *p* value should be higher than the chosen threshold called significance level. Typical significance level of 0.05 was chosen.

The test statistics was defined as $F_{s_1}(x)$- doses at angle Θ and $F_{s_2}(x)$- doses at angle 360˚- Θ.

Kolmogorov–Smirnoff test was used to compare the MatriXX measured doses at angles Θ and 360˚- Θ. The average *p* value was 0.84 and average *D* value was 0.028 .The minimum *p* value was less than 0.0001, at which the null hypothesis that the MatriXX measured doses are symmetrical can be rejected.

The Monaco calculated doses at angles Θ and 360˚- Θ were also compared. The average *p* value was 0.97, the average *D* value was 0.019, and the minimum *p* value was 0.73, at which the hypothesis of TPS-calculated doses symmetry can't be rejected.

2.4.5. Correction factor set based on film measurements

For the LUT based on film measurement a single correction factor was created for all detectors at a given gantry angle. The correction factors were calculated for angles from 0˚ to 180˚ and mirrored for angles 180˚-360˚.The average dose D^{meas} from the 4 central detectors at every angle were feed into Python3 along with the film measured doses and correction factors *C*(Θ) were calculated according to eq. (2.2) and (2.3).

2.4.6. Correction factor sets based on Monte Carlo simulation

The TPS calculated dose distributions in the plane of the chamber measured readings were interpolated to a matrix with dose values located coincident with the center of each ion chamber in the of the OmniPro I'mRT software, after that they were exported in the form of ASCII files, which feed into Python3.

For all LUTs the doses were normalized with a correction factor calculated in Python3, individual normalization factor for every chamber was not used, because the chamber reading uncertainty and the uncertainty in the gantry position may lead to inaccurate normalization factors. Furthermore the MatriXX is designed to measure beams at normal incidence to the MatriXX, at normal incidence the effective angle and effective point of measurement are the same for all chambers and the beam passes the same build-up material. Calculation of the normalization factor was done in 3 steps. Example for step 1 and 2 is shown in fig.2.9.

1. Symmetrization on x and y axis for the TPS calculated doses at gantry angle 0˚ according to equation:

$$D_{i,j}^{TPS,sym} = (D_{i,j}^{TPS} + D_{i,j_{max}+1-j}^{TPS} + D_{i_{max}+1-i,j}^{TPS} + D_{i+1-i,j_{max}+1-j}^{TPS})/4 \qquad (2.7)$$

where $D_{i,j}^{TPS}$ is the dose calculated by the TPS corresponding to the detector at located at row *i* and column *j*.

2. Symmetrization on x and y axis for the MatriXX measured doses at gantry angle 0˚acording to equation:

$$D_{i,j}^{meas,sym} = (D_{i,j}^{meas} + D_{i,j_{max}+1-j}^{meas} + D_{i_{max}+1-i,j}^{meas} + D_{i+1-i,j_{max}+1-j}^{meas})/4 \qquad (2.8)$$

where $D_{i,j}^{TPS}$ is the measured dose by detector at position *i,j*

3. Calculation of the normalization factor as the ratio of $D^{meas,sym}$ to $D^{TPS,sym}$:

$$N = \sum_{i=1}^{32} \sum_{j=j_{min}}^{j_{max}} \frac{1}{n} \frac{D_{i,j}^{meas,sym}}{D_{i,j}^{TPS,sym}} \qquad (2.9)$$

where *n* is the number of detectors

In order to exclude the corners of the MatriXX (there are no detectors and the dose is interpolated via the MatriXX software) from the calculation the summation limits are:

If: $i = 1$ or $i = 32$ then $j_{max}=31$ and $j_{min}=2$

If: $i \neq 1$ and $i \neq 32$ then $j_{max}=32$ and $j_{min}=1$

Value of 1.004 was calculated for the factor.

To calculate the correction factors the summed measurements and the calculated doses were symmetrized on the Y axis:

$$D_{i,j}^{TPS,sym} = (D_{i,j}^{TPS} + D_{i_{max}+1-i,j}^{TPS})/2 \quad (2.10)$$

and

$$D_{i,j}^{meas,sym} = (D_{i,j}^{meas} + D_{i_{max}+1-i,j}^{meas})/2 \quad (2.11)$$

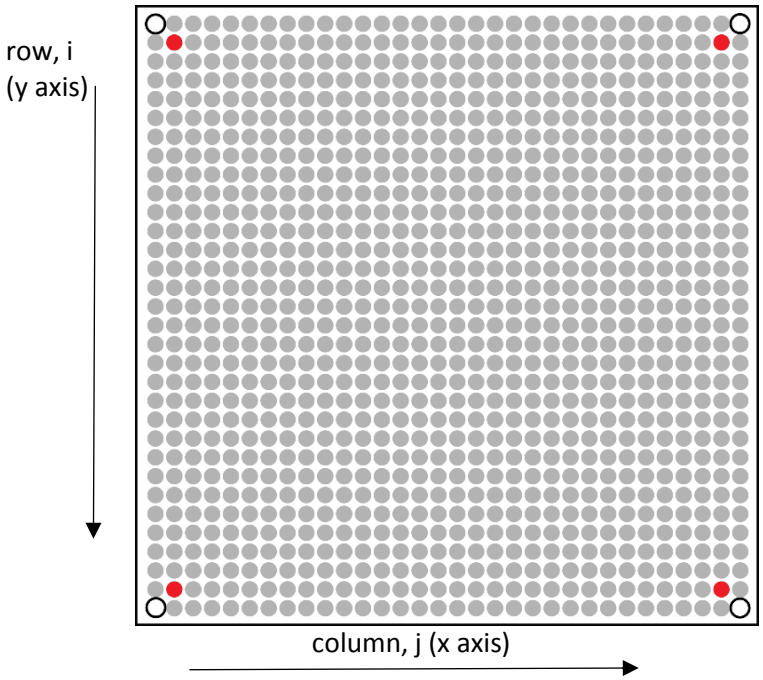

Figure 2.9. *- Symmetrization. One gray circle represent MatriXX detector. TheMatriXX doses at the detectors position indicated by red were averaged. This symmetrical averaging on the x and y axis was done for all measured and TPS calculated doses at angle 0˚.The corners of the MatriXX, where there are no detectors, are indicated with black annulus (ring-shaped object).*

Symmetrization on the Y axis assures that daily variations in the beam flatness (on the Y axis) would not affect the factors. The correction factors at different LUTs differ by the way the doses corresponding to the detector at position *i,j* on the chamber array were averaged, as shown with some examples on fig. 2.10.

At the corners of the MatriXX (see fig. 2.9) it was found out that the dose is consistently overestimated with about 1.2% at angle 0˚,so at 0˚ correction factor was calculated only at the MatriXX corners. At all other angles the correction factors at the corners were calculated without taking into account the neighbor detectors. Thus points with *i,j* coordinates (1,1),(1,32), (32,1) and (32,32) are excluded from the summations eq, (2.12),(2.13),(2.17),(2.18).

Here are listed all created LUTs for 6MV beams and the way they were created:

a) LUT "1x1"

For the first LUT "1x1" no averaging was done:

$$\overline{D}_{i,j}^{meas,sym} = D_{i,j}^{meas,sym} \tag{2.12}$$

and

$$\overline{D}_{i,j}^{TPS,sym} = D_{i,j}^{TPS,sym} \tag{2.13}$$

b) LUT "3x1"

For the second LUT the dose at the 2 nearest detectors on the same column were taken into account, except on the edges in the y axis, where only the dose was averaged over the detector and the nearest detector on the same column. At the MatriXX corners $\overline{D}_{i,j}^{TPS,sym}$ and $\overline{D}_{i,j}^{meas,sym}$ were calculated according to equations (2.12) and (2.13):

$$\overline{D}_{i,j}^{meas,sym} = \frac{1}{i_{max} - i_{min} + 1} \sum_{i_{min}}^{i_{max}} D_{i,j}^{meas,sym} \tag{2.14}$$

and

$$\overline{D}_{i,j}^{TPS,sym} = \frac{1}{i_{max} - i_{min} + 1} \sum_{i_{min}}^{i_{max}} D_{i,j}^{meas,sym} \tag{2.15}$$

where:

$i_{min} = i - 1$ and $i_{max} = i + 1$;

If: $i - 1 = 1$ and $(j = 1 \text{ or } j = 32)$ then $i_{min} = 2$;

If: $i + 1 = 32$ and $(j = 1 \text{ or } j = 32)$ then $i_{max} = 31$;

If: $i - 1 = 0$ then $i_{min} = 1$;

If: $i + 1 = 33$ then $i_{max} = 32$.

c) LUT "32x1"

The doses at every column were averaged. In eq. (2.14), (2.15) i is:

$i_{min} = 1$ and $i_{max} = 32$;

If: $i = 1$ or $i = 32$ then $i_{min} = 2$ and $i_{max} = 31$.

At the MatriXX corners $\overline{D}_{i,j}^{TPS,sym}$ and $\overline{D}_{i,j}^{meas,sym}$ were calculated according to equations (2.12) and (2.13).

For the other sets the MatriXX doses calculated by the TPS, were also averaged over angles Θ and 360 - Θ. The MatriXX model in the TPS is symmetrical so angle symmetrization should improve the accuracy of the TPS calculation:

$$D_{i,j}^{TPS,sym\,\Theta}(\Theta) = D_{i,j}^{TPS,sym}(\Theta) + D_{i,j_{max}+1-j}^{TPS,sym}(360^{\circ} - \Theta) \tag{2.16}$$

d) LUT "1x1sym"

For the first LUT "1x1sym" no averaging was done (the value of $\overline{D}_{i,j}^{meas,sym}$ is the same as for"1x1", but the value of $\overline{D}_{i,j}^{TPS,sym}$is not the same).

$$\overline{D}_{i,j}^{meas,sym} = D_{i,j}^{meas,sym} \tag{2.17}$$

and

$$\overline{D}_{i,j}^{TPS,sym} = D_{i,j}^{TPS,sym\Theta} \tag{2.18}$$

e) LUT "3x1sym"

The same calculation was performed as for LUT "3x1", but first TPS - angle symmetrization was performed.

f) LUT"3x3sym"

For the LUT"3x3sym" the doses were averaged over a window corresponding to 9 detectors. On the edges window corresponding to the 6 detectors was used. On the corners eq. (2.17) and (2.18) were used:

$$\overline{D}_{i,j}^{meas,sym} = \frac{1}{(i_{max} - i_{min} + 1)(j_{max} - j_{min} + 1)} \sum_{j_{min}}^{j_{max}} \sum_{i_{min}}^{i_{max}} D_{i,j}^{meas,sym} \tag{2.19}$$

and

$$\overline{D}_{i,j}^{TPS,sym} = \frac{1}{(i_{max} - i_{min} + 1)(j_{max} - j_{min} + 1)} \sum_{j_{min}}^{j_{max}} \sum_{i_{min}}^{i_{max}} D_{i,j}^{TPS,sym\Theta} \tag{2.20}$$

where:

$i_{min} = i - 1$ and $i_{max} = i + 1$; $j_{min} = i - 1$ and $j_{max} = i + 1$;

If: $i - 1 = 1$ and $(j = 1$ or $j = 32)$ then $i_{min} = 2$; If: $j - 1 = 1$ and $(i = 1$ or $i = 32)$ then $j_{min} = 2$;

If: $i + 1 = 32$ and $(j = 1$ or $j = 32)$ $i_{max} = 31$; If: $j + 1 = 32$ and $(i = 1$or $i = 32)$ then $j_{max} = 31$;

If: $i - 1 = 0$ then $i_{min} = 1$; If: $j - 1 = 0$ then $j_{min} = 1$;

If: $i + 1 = 33$ then $i_{max} = 32$; If: $j + 1 = 33$ then $j_{max} = 32$.

g) LUT “5x5sym

For LUT “5x5sym” a window corresponding to 25 detectors was chosen, except on the edges where window corresponding to 9 or 6 detectors was chosen. The same equations were used as for LUT “3x3sym”.The limits of summation near the edges (2 detectors till the edge) were as for LUT”3x3sym”.For all other doses the limits were:

$i_{min} = i - 2$ and $i_{max} = i + 2$ $\qquad$ $j_{min} = j - 2$ and $j_{max} = j + 2$

h) LUT “32x1sym”

The doses at every column were averaged as for LUT”32x1”.In eq. (2.15) substitutions done: $\overline{D}_{i,j}^{TPS,sym} \mapsto D_{i,j}^{TPS,sym\Theta}$

At the MatriXX corners $\overline{D}_{i,j}^{TPS,sym}$ and $\overline{D}_{i,j}^{meas,sym}$ were calculated according to equations (2.16) and (1.17).

i) LUT”32x1sym_and_1x1sym”

The LUT”32x1sym_and_1x1sym” was generated via different approaches at different gantry angles. In the ranges [90˚- 95˚] and [265˚-270˚] the mean absolute deviation of the detectors response is underestimated by the TPS calculation as shown on fig.2.15. At angles in the ranges [90˚-95˚] and [265˚-270˚] $\overline{D}_{i,j}^{TPS,sym}$ and $\overline{D}_{i,j}^{meas,sym}$were calculated as for LUT”1x1sym” (angel symmetrized, without averaging). For all other angles equations as LUT”32x1sym” (angel symmetrized, averaged over column).

All LUTs correction factors were created by dividing the averaged calculated doses at each ion position to the averaged MatriXX measured doses:

$$C_{i,j}(\theta) = N \frac{\overline{D}_{i,j}^{TPS,sym}(\theta)}{\overline{D}_{i,j}^{meas,sym}(\theta)} \qquad (2.21)$$

For 10 MV and 15 MV energies were created LUTs ”32x1sym_and_1x1sym”. See Appendix A.3 for the code used to generate the correction factors along with the normalization factor.

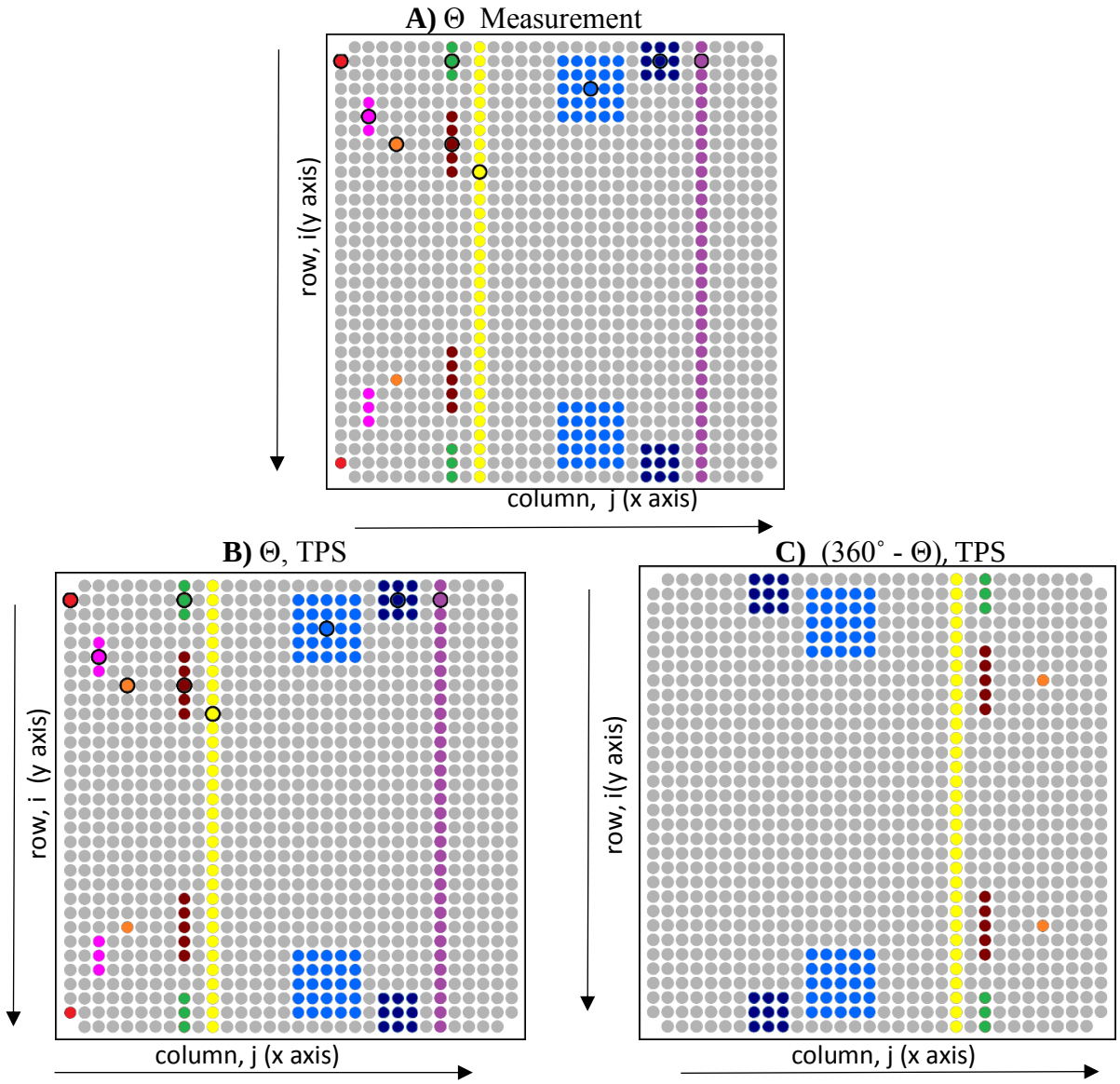

Figure 2.10. *- Examples for the different ways correction factor was created for every LUT based on Monaco calculation. One circle represent MatriXX detector. The doses used for the calculation of a single correction factor at position shown by the black annulus for a given LUT (at angle Θ) is the average of the chamber doses of the same color as the color within the annulus.* ***A*** *MatriXX-measured doses.* ***B*** *Monaco calculated doses.* ***C*** *Monaco calculated doses. For example the doses for the calculation of the correction factor correcting for chamber at position row=6 and column = 3(the position is indicated by the black annulus) for the LUT"3x1" is the average dose of all detectors with the same pink color (The ratio of the 6 measured to the 6 calculated doses were used for the calculation). "1x1 ","3x1", "32x1 ", "1x1sym", "3x1sym", "3x3sym ", "5x5sym ", "32x1sym"*

2.5. Correction factors validation

The 6 MV correction factors were statistically analyzed via Python3 and verified with patient plans, by comparing calculated doses by the treatment planning system to MatriXX measured doses using gamma criterion.

2.5.1. Variations of the MatriXX-measured doses compared to the variations of the Monaco-calculated doses

At angles at which the average measured dose or its variations differ significantly from the Monaco calculated average dose or its variation, the correction factors are certainly needed. Ideally (when no correction factors are needed) these differences will be result of uncertainties associated with the MatriXX measurements and the Monaco calculation. To evaluate at which angels the MartiXX intrinsic dependency is significant the mean measured and calculated dose were calculated along with their standard deviation and mean absolute deviation for 6 MV beam were used (including at angle 0˚ to serve as a baseline). The relative standard STD_r and mean deviations MD_r were calculated on the x and y axes for the Monaco-calculated and MatriXX measured doses. Moreover the validity of the assumptions that the same correction factor can be applied to all detectors on a given row or column were investigated.

The Monaco-calculated doses were angle-symmetrized according to equation (2.14) prior to the calculation, because the tests for symmetry indicate that the measured doses at angle Θ and at angle 360˚- Θ come from the same distribution. Furthermore the statistical tests indicate that MatriXX measured doses at angle Θ and at angle 360˚- Θ don't come from the same distribution. MatriXX measured doses were normalized with the normalization factor described at chapter 2.4.6.

In order to exclude the corners of the MatriXX from the calculation the lower limits and the upper limits of the summations in eq. (2.22) to (2.31) are:

If: $j = 1$ *or* $j = 32$ then $i_{max}=31$ and $i_{min}=2;$

If: $j \neq 1$ *or* $j \neq 32$ then $i_{max}=32$ and $i_{min}=1;$

If: $i = 1$ *or* $i = 32$ then $j_{max}=31$ and $j_{min}=2;$

If: $i \neq 1$ *or* $i \neq 32$ then $j_{max}=32$ and $j_{min}=1$.

The relative standard STD_r and mean deviations MD_r were calculated on the x and y axes for the Monaco-calculated and MatriXX measured doses.

The relative mean and standard deviations on the y axis for the Monaco calculated ($STD_r^{y,tps}$ and $MD_r^{y,tps}$) and MatriXX measured ($STD_r^{y,meas}$ and $MD_r^{y,meas}$) distributions at angle Θ were calculated as follows:

The average dose on column *j* is given by:

$$\bar{D}_j^y(\Theta) = \frac{1}{i_{max} - i_{min} + 1} \sum_{i=i_{min}}^{i_{max}} D_{i,j}. \tag{2.22}$$

Standard deviation is calculated as:

$$STD_r^y(\Theta) = \sqrt{\frac{\sum_{j=j_{min}}^{j_{max}} \sum_{i=i_{min}}^{i_{max}} (D_{i,j} - \bar{\boldsymbol{D}}_{\boldsymbol{j}}^{\boldsymbol{y}})^2}{n-1}}. \tag{2.23}$$

where *n* is the total number of detectors

Mean absolute deviation is calculated as:

$$MD_r^y(\Theta) = \frac{\sum_{j=j_{min}}^{j_{max}} \sum_{i=i_{min}}^{i_{max}} |D_{i,j} - \bar{\boldsymbol{D}}_{\boldsymbol{j}}^{\boldsymbol{y}}|}{n}. \tag{2.24}$$

The relative mean and standard deviations on the x axis for the Monaco-calculated ($STD_r^{x,tps}$and $MD_r^{x,tps}$) and measured($STD_r^{x,meas}$ and $MD_r^{x,meas}$) were also calculated:
The average dose on row *i* is given by:

$$\bar{D}_i^x(\Theta) = \frac{1}{j_{max} - j_{min} + 1} \sum_{j=j_{min}}^{j_{max}} D_{i,j}\,. \tag{2.25}$$

Standard deviation is calculated as:

$$STD_r^x(\Theta) = \sqrt{\frac{\sum_{j=j_{min}}^{j_{max}} \sum_{i=i_{min}}^{i_{max}} (D_{i,j} - \bar{\boldsymbol{D}}_{\boldsymbol{i}}^{\boldsymbol{y}})^2}{n-1}}. \tag{2.26}$$

Mean absolute deviation is calculated as:

$$MD_r^x(\Theta) = \frac{\sum_{j=j_{min}}^{j_{max}} \sum_{i=i_{min}}^{i_{max}} |D_{i,j} - \bar{\boldsymbol{D}}_{\boldsymbol{j}}^{\boldsymbol{y}}|}{n}. \tag{2.27}$$

To assess the validity of the assumption that the same correction factor can be applied to all detectors on the same column the standard deviation and the mean deviation of the ratio R^y of a correction factors without the assumption to the factors with the assumption was calculated at each angle:

$$R_{i,j}^{y}(\Theta) = \frac{C_{i,j}^{\Theta}(not\ averaged)}{C_{i,j}^{\Theta}(avereged\ over\ column)} \tag{2.28}$$

where:

$C_{i,j}^{\Theta}(not\ averaged)$ were calculated as for LUT"1x1", but including calculation at 0˚.

$C_{i,j}^{\Theta}(avereged\ over\ column)$ were calculated as for LUT"32x1", but including calculation at 0˚.

The assumption that the same correction factor can be applied to all detectors on the same row was investigated by calculating the standard deviation and the mean deviation of the ratio R^x of a correction factors without the assumption to the factors with the assumption.

$$R_{i,j}^{x}(\Theta) = \frac{C_{i,j}^{\Theta}(not\ averaged)}{C_{i,j}^{\Theta}(avereged\ over\ row)} \tag{2.29}$$

where:

$C_{i,j}^{\Theta}(not\ averaged)$ were calculated as for LUT"1x1", but including calculation at 0˚.

$C_{i,j}^{\Theta}(avereged\ over\ row)$ were calculated with eq. (2.21), (including calculation at 0˚)

where :

$$\overline{D}_{i,j}^{meas,sym} = \frac{1}{j_{max}} \sum_{j=i_{min}}^{j_{max}} D_{i,j}^{meas,sym\Theta} \tag{2.30}$$

and

$$\overline{D}_{i,j}^{TPS,sym} = \frac{1}{j_{max}} \sum_{j=i_{min}}^{j_{max}} D_{i,j}^{TPS,sym\Theta} \tag{2.31}$$

The MatriXX measured normalized mean doses and TPS calculated mean doses at different angles are shown on fig. 2.11 and 2.12. The correction factors should transform the measured dose profile to identical to the TPS-calculated profile.

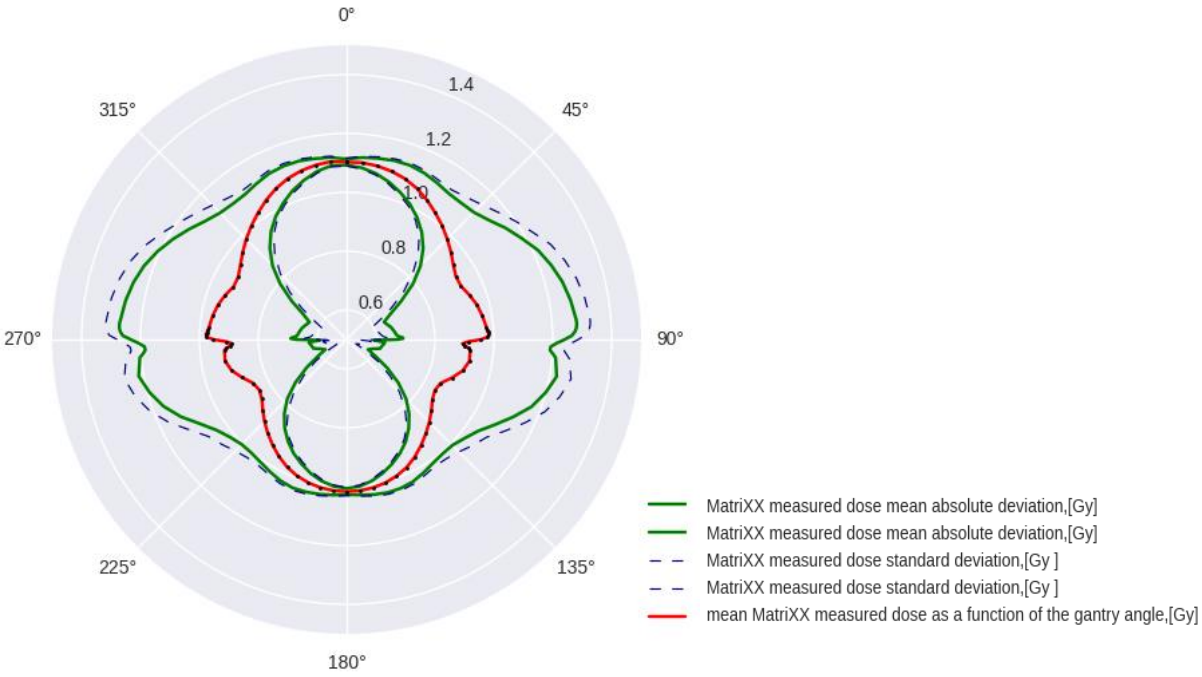

Figure 2.11. *- 6MV Measured doses: mean dose, standard deviation and mean absolute deviation at different angles*

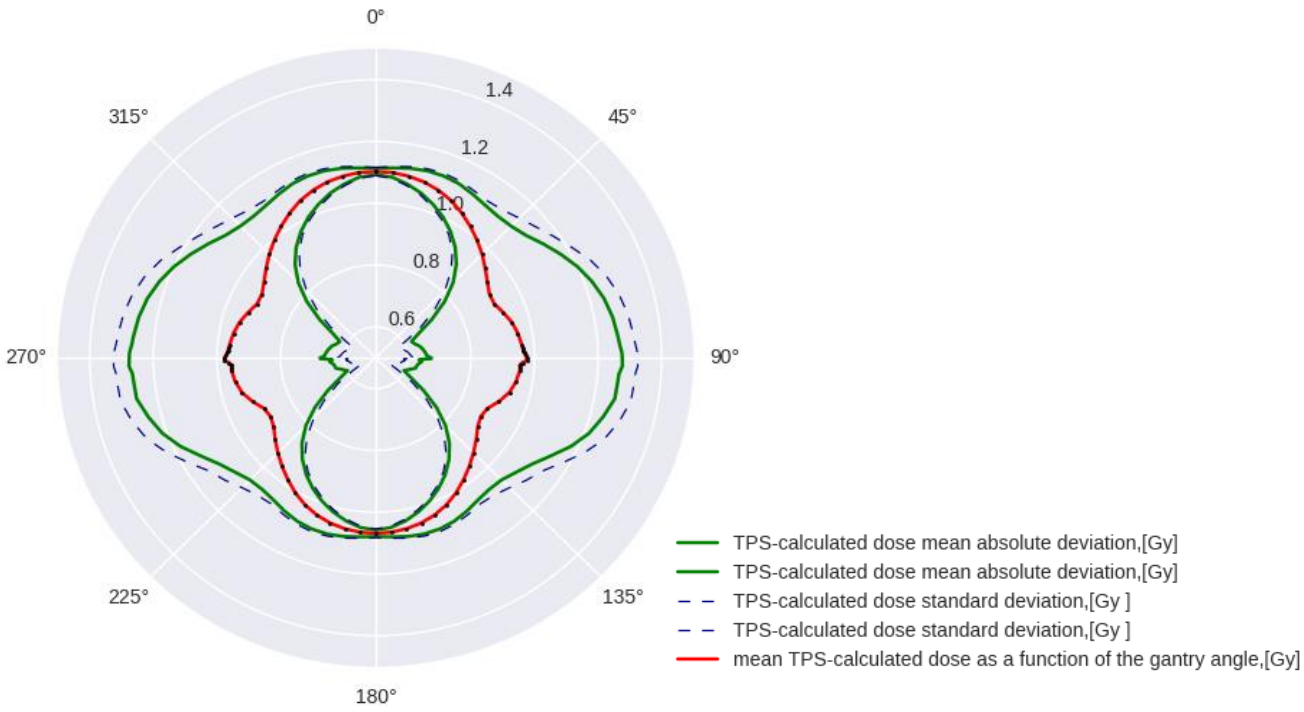

Figure 2.12. *- 6 MV TPS calculated doses: mean dose, standard deviation and mean absolute deviation at different angles*

On figure 2.13 and 2.14 are shown the relative standard and mean deviations on the x and y axes for the Monaco-calculated and MatriXX measured doses. They are calculated according to equations (2.22), (2.23), (2.24), (2.25), (2.26), (2.27).

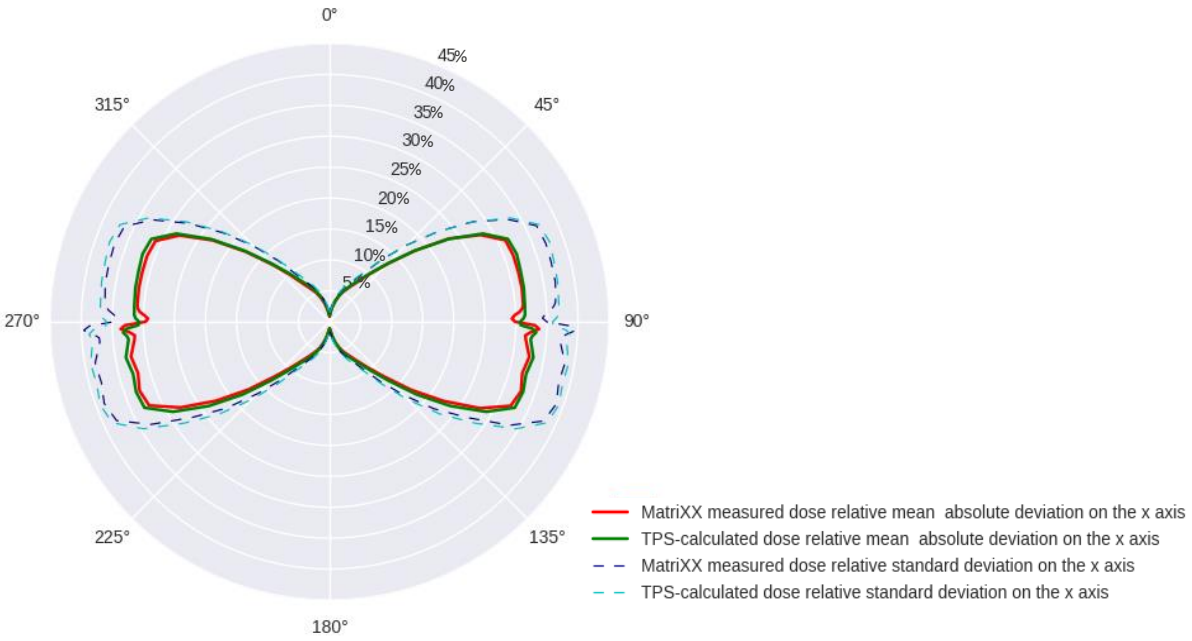

Figure 2.13. *- 6MV Calculated doses and measured doses relative standard deviation and mean absolute deviation on the x axis at different angles*

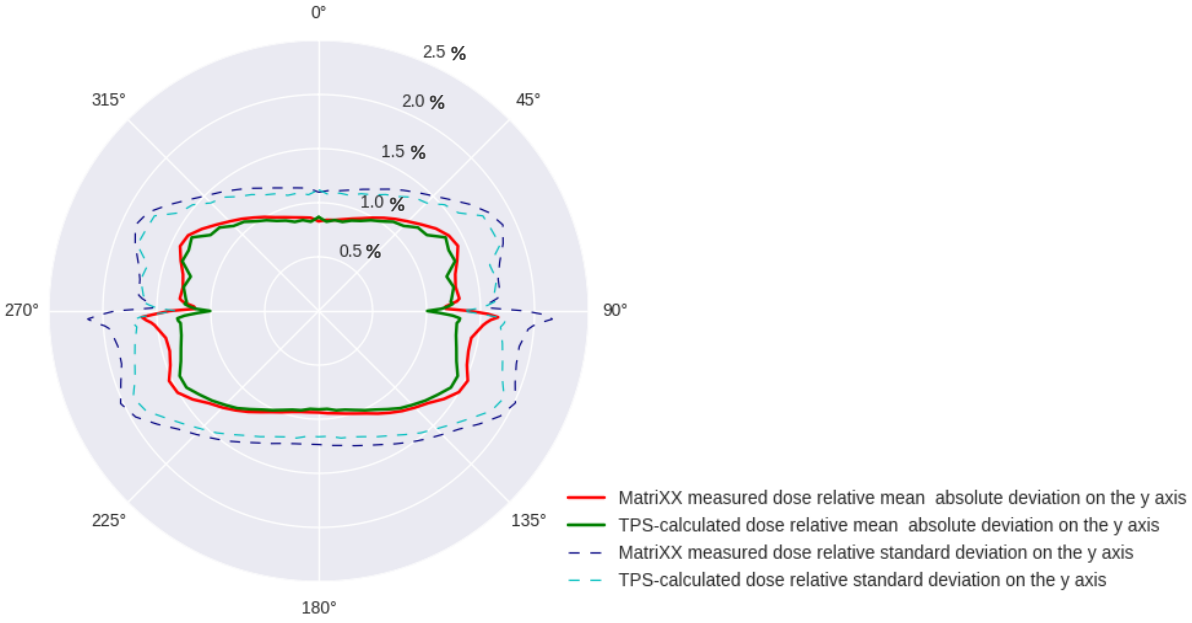

Figure 2.14. *- 6 MV Calculated doses and measured doses relative standard deviation and mean absolute deviation on the y axis at different angles*

The measured and calculated doses on the x axis vary much more than the measured doses on the y axis. This can't be contributed to changes in the detectors response at different angles (see 2.3.2). The assumption that the same correction factor can be applied to all detectors on the same row (x axis) or column (y axis) was further investigated. The standard deviation and the mean deviation of the ratio of a correction factors ($C_{i,j}^{\theta}$) without the assumption to the factors with the assumption calculated according to eq. (2.22), (2.23), (2.24), (2.25), (2.26), (2.27) are shown in fig. 2.15.

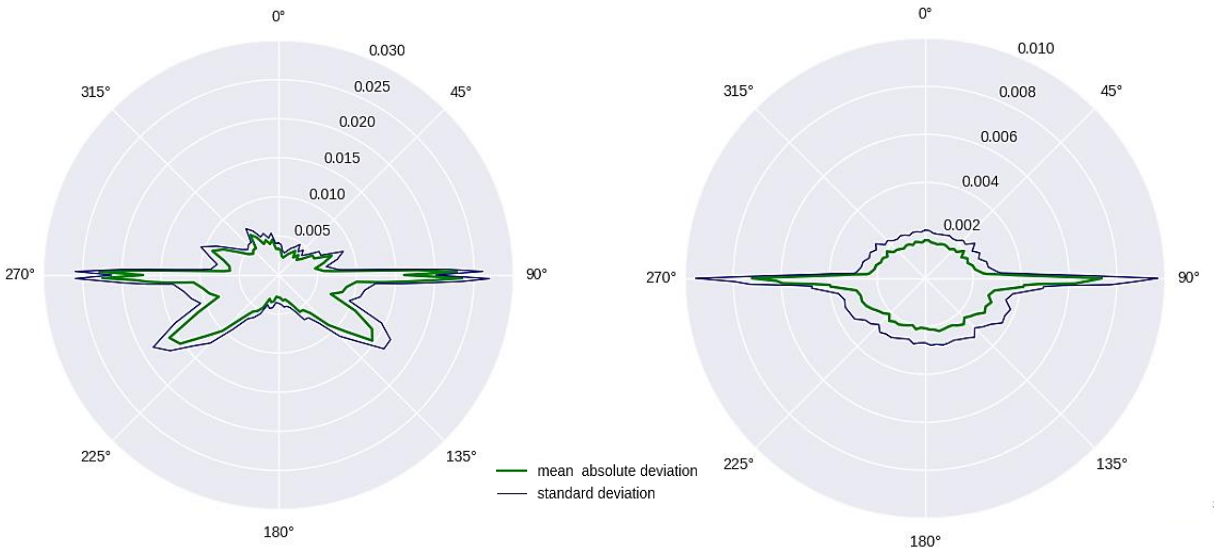

Figure 2.15. *- Standard deviation and mean absolute deviation of the ratio:* ***A)*** $C_{i,j}^{\Theta}$*(not averaged)/* $C_{i,j}^{\Theta}$*(averaged over row).* ***B)*** $C_{i,j}^{\Theta}$*(not averaged)/* $C_{i,j}^{\Theta}$*(averaged over column)at different angles*

At 0˚ the relative standard deviation and absolute deviation are result of the uncertainties associated with: Monaco calculation, detectors responses, gantry angle and beam flatness. At angles where the deviations of the ratio $C_{i,j}^{\Theta}$*(not averaged)/* $C_{i,j}^{\Theta}$*(averaged over row),* exceeds significantly the deviations at 0˚ one correction factor for each row should not be used. For the majority of angles the mean and standard deviations of this ratio is more than two times higher than the deviations at 0˚.

If the ratio $C_{i,j}^{\Theta}$*(not averaged)/* $C_{i,j}^{\Theta}$*(averaged over column),* exceeds significantly the deviations at 0˚ one correction factor for each column should not be used. Only for angles in the range 85˚-95˚ and 265˚-270˚ the mean and standard deviations of this ratio is more than one and a half times higher than the deviations at 0˚(standard deviation at 0˚ is about 0.2%).

2.5.2. Correction factors verification

The user created 6MV LUTs were compared by taking measurements with the MatriXX applying correction factors, and comparing the uncorrected and corrected measurements against the calculated patient plans exported from the treatment planning system using gamma analysis (2% dose difference, 2 mm distance to agreement and 3% dose difference, 3 mm distance to agreement with 10% threshold). Doses were interpolated to a 1 mm grid size with the Omnipro software before comparison.

The 6 MV custom correction factors were verified with 30 patient plans. The results of no correction factor and applying custom correction factors to the patient plans are given in Tables 2.3 and 2.4 The average percent of pixels passing gamma criteria are given when no correction factor is used and when the custom created LUTs are used along with: absolute mean deviation,

standard deviation, minimum and maximum improvement of the passing percent. The tables are sorted by column "improvement of gamma" in descending order.

Table 2.3. - Applying custom correction factors and no correction factors to 6 MV patient plans, gamma criteria 3%, 3mm.

Correction	**Improvement of gamma 3%,3mm(from no correction)**	**Gamma 3%,3mm**	**Absolute mean deviation**	**Standard deviation**	**Minimum**	**Maximum**
no correction	-	93.33	3.47	4.2	-	-
32x1sym_and_1x1sym	+4.08	97.41	3.16	4.03	-0.63	+13.96
32x1sym	+4	97.33	3.16	4.05	-0.7	+13.96
3x1sym	+3.98	97.31	3.16	4.04	-0.75	+13.89
32x1	+3.98	97.31	3.18	4.05	-0.78	+13.94
3x3sym	+3.98	97.31	3.18	4.07	-0.87	+13.99
1x5sym	+3.98	97.31	3.16	4.04	-0.76	+13.94
1x1sym	+3.97	97.3	3.15	4.04	-0.77	+13.89
3x1	+3.97	97.3	3.17	4.05	-0.81	+13.89
5x5sym	+3.97	97.3	3.17	4.06	-0.86	+14.01
1x1	+3.69	97.02	2.83	3.75	-0.83	+13.86
Film	+2.69	96.02	3.17	4.3	-3.3	+14.34

Table 2.4. - Applying custom correction factors and no correction factors to 6 MV patient plans, gamma criteria 2%, 2mm.

Correction	**Improvement of gamma 2%,2mm(from no correction)**	**Gamma 2%,2mm**	**Absolute mean deviation**	**Standard deviation**	**Minimum**	**Maximum**
no correction	-	82.55	5.09	6.67	-	-
32x1sym_and_1x1sym	+4.96	87.51	3.19	5.24	-2.19	+23.57
32x1sym	+4.95	87.5	3.26	5.3	-2.3	+23.57
32x1	+4.94	87.49	3.27	5.28	-2.17	+23.5
3x1	+4.92	87.47	3.27	5.23	-2.36	+23.11
3x1sym	+4.92	87.47	3.3	5.24	-2.49	+23.12
1x5sym	+4.92	87.47	3.3	5.27	-2.52	+23.27
3x3sym	+4.91	87.46	3.31	5.27	-2.56	+23.23
1x1	+4.9	87.45	3.27	5.24	-2.39	+23.17
5x5sym	+4.9	87.45	3.28	5.25	-2.66	+23.19
1x1sym	+4.89	87.44	3.3	5.29	-2.56	+23.35
Film	+2.22	84.77	4.48	8.11	-21.18	+26.76

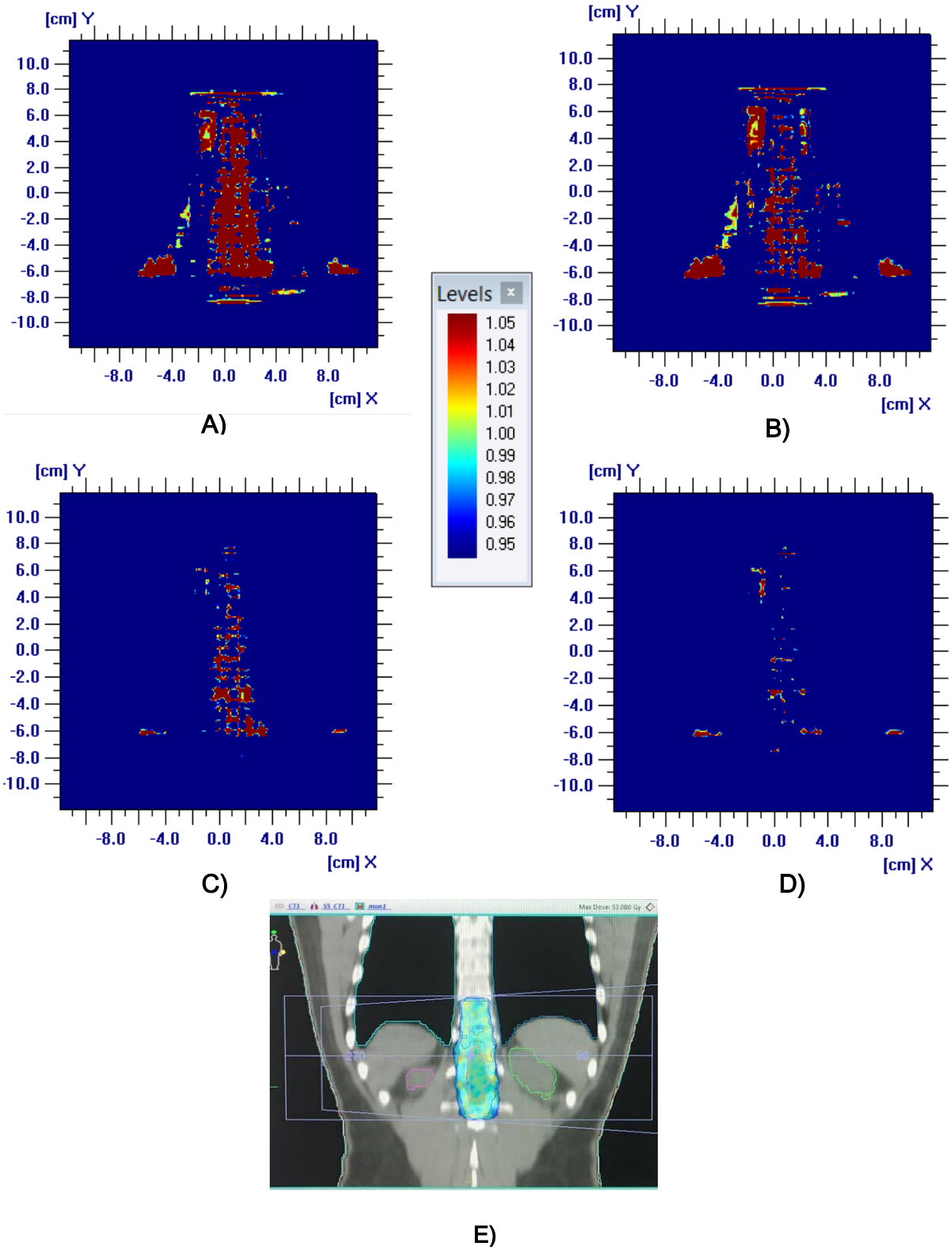

Figure 2.16. *- Gamma map before and after correction with LUT"1x1_and_32x1". Improvement of gamma close to the average improvement was observed for the given patient plan – ependimoma of spinal cord Th11-12.* ***A)*** *gamma 2%, 2mm before correction was: 80.68%* ***B)****after correction gamma 2%, 2mm was: 86.15%* ***C)*** *gamma 3%, 3 mm before correction was: 95.47%* ***D)****after correction gamma 3%, 3mm was: 98.66%* ***E)****The patient plan represented in the TPS.*

The verification of the correction factors using patient plans shows that when applied they improve the percent of pixels passing a gamma criteria. For both the "32x1_and_1x1" correction factors showed the highest passing rates, followed by "32x1sym". In average, for the 30 analyzed plans, the percent of points passing a gamma criteria 2% 2mm was increased from 82,55% to 87,51% and the percent of points passing a gamma criteria 3% 3mm was increased from 93,33% to 97,41%. In general, the results are in good agreement with the data obtained by other researchers, such as Wolfsberger L. D at all [31].

When no correction factors were applied the results were worst. All LUTs based on Monaco calculation yielded similar results. The LUT based on film measurements didn't improve gamma as much as the other LUTs and also its improvement of gamma is much more variable.

Depending on plan design, the result may be dramatically improved or get slightly worth. The correction factors in LUT"1x1_and _32x1" improved the passing rate by 13,96% for gamma 2% 2mm and by 23,57% for gamma 3% 3mm.The minimum gamma improvement for all LUTs was scored on the-same plan, the degradation may be due to variety of factors. A possible source for disagreement between measured and calculated distributions is the MatriXX spatial resolution. Since the ion chambers are 7.62 mm apart, when the MatriXX is irradiated with fields less than 7.62 mm only one chamber will be irradiated, furthermore only part of the chamber may be irradiated, because its active area is 4.5 x 5 mm with a chamber volume of 0.08 cm^2. This could lead to inaccuracy in the dose measured for small fields. There is also an inconsistency between actual and planned position of MLC-leaves during VMAT delivery. In that case accuracy of MLC positioning depends on many factors, such as last MLC calibration parameters, plan modulation degree, and synchronizing between Gantry rotation speed and MLC movement speed. According vendor specification accuracy of Agility MLC positioning should be less than 1 mm. In case the plans, where mostly Gantry angles are close to 90˚ or 270˚, the uncertainty of the angle sensor position ±0.5° may decrease the passing rate because of strong angular dependency changing.

2.6. Correction factors distribution

The gamma analysis and the statistical analysis show that the optimum LUT is"32x1_and_1x1". Histogram of all LUT "32x1_and_1x1"correction factors for 6MV is shown on fig. 2.17 and their angular distribution on fig. 2.18

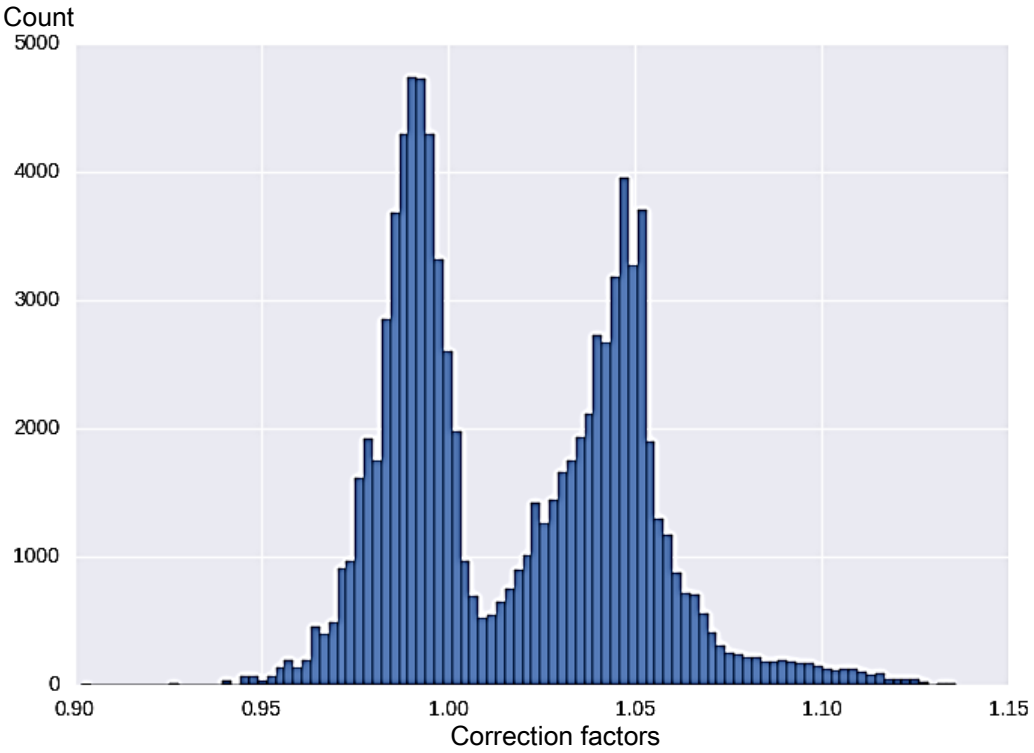

Figure 2.17. *- All LUT"32x1and1x1" 6MV correction factors.*

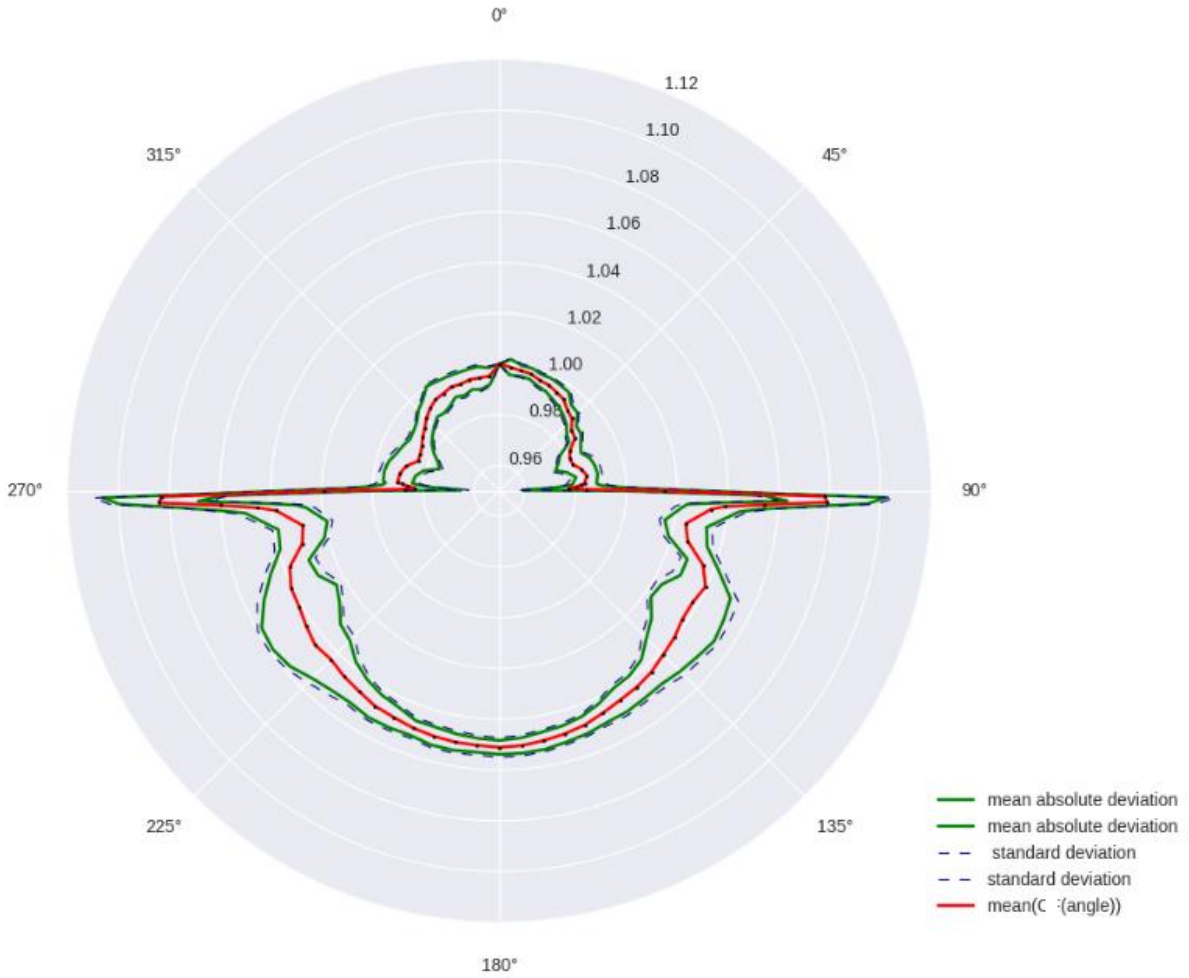

Figure 2.18. *- Mean value, standard and mean absolute deviations of the correction factors at different angles for 6MV.*

Correction factors for 10MV and 15MV beams were created following the same procedure used to create LUT"1x1_and_32x1" for 6 MV beam. On figure 2.19 are shown the mean correction factors at energy 6, 10 and 15 MV and their standard deviation about the mean for angles 0˚-180˚.

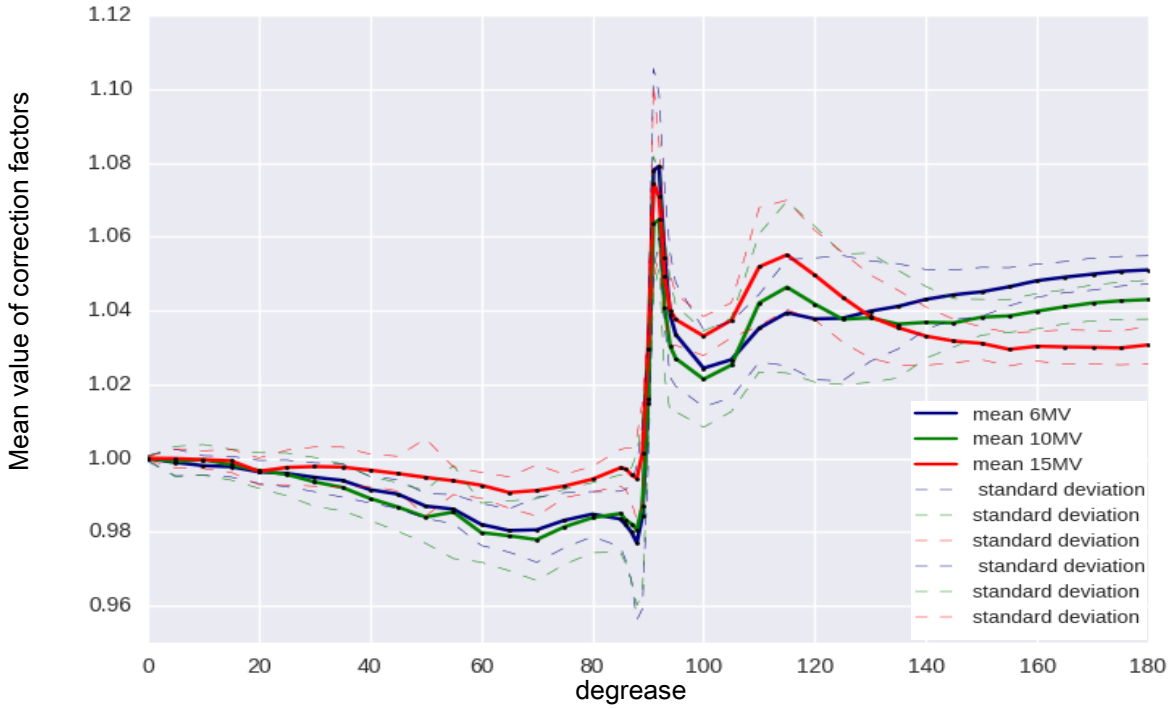

Figure 2.19. *- Mean value and standard deviations of the correction factors (LUT"1x1_and_32x1"), at angles 0˚-180˚ for energies 6, 10 and 15 MV.*

Figure 2.19 demonstrate the large variability in chambers response, particularly as the central axis of the radiation field gets closer to parallel position with respect to the ion chamber plane. When the incoming radiation is parallel to the plane where the ion chambers are situated, most of the photons will pass through the air-filled chambers instead through the water-equivalent build-up material. Furthermore, the MatriXX ion chambers are designed to measure radiation with its central axis perpendicular to MatriXX orientation, when used in such orientation the effective point of measurement is situated on the front surface of the chamber. When the radiation field is not parallel to the MatriXX, the effective point of measurement changes its location. The change of the effective point of measurement is nearly the same for all detectors on the same row, also the beam has to pass practically the same build-up to reach the detectors on the same column. The correction factors are subject to effects created by the high density plane of electronics below the plane of ion chambers, which may contribute to the MatriXX inherent angular dependency. In addition, the figures support that correction factors have to be derived from a full 360° measurement, since the measured doses are asymmetric, however for the purpose of QA a symmetric profile can be used. Also the central four detectors don't represent the average response of all detectors.

CONCLUSION

In this study the angular dependency of the MatriXX detectors was investigated and an efficient methodology for creation of correction factors was developed.

In the first part of the work the importance of efficient quality control program in radiotherapy was reviewed. The importance of delivering reliably and reproducibly dose distribution conforming to the tumor was shown. Sources of uncertainty in film and ion chamber measurements and their theoretical back ground of this was reviewed. The principles based on which medical accelerator works, along with the sources that can influence their output constancy were shown. The basic principles of the Monte Carlo calculation algorithm and the algorithm utilized by the Monaco were displayed. The accuracy requirements in radiotherapy were reviewed. Furthermore previous attempts for patient individual VMAT and IMRT plan verification attempts were described.

In the second part the following experiments were performed:

- Two identical Synergy accelerators were calibrated as recommended at TRS-398.
- The MatriXX warm up behavior was investigated and the standard deviation of the MatriXX detectors response calculated.
- It was shown that the accelerator output constancy dependence from the gantry angle is within acceptable tolerance.
- Correction factor sets for 6MV, 10MV and 15 MV beams were created. The MatriXX ion chamber array was irradiated from 88 angles. Reference dose distributions were obtained via Monte Carlo calculation and independently from the calculation – with the radoichromic film measurements.
- The angular dependency of the MatriXX was statistically analyzed. It was shown that there is asymmetry between MatriXX measured doses for incident radiation from 0˚-180˚ and 180˚-360˚.In addition it was shown that a correction factor unique for each row can be used for all angles, with the exclusion of angles in the ranges 90˚ - 95˚ and 265˚ - 270˚ where unique factor for each detector give optimal results.
- The correction factor sets for 6MV beams were validated by comparing the measured doses before and after applying angle correction to Monaco calculated doses. The gamma passing rate was improved with all correction factors. The correction factors in LUT"1x1_and _32x1" improved the passing rate more than all other correction factors, which was also the expected result from the statistical analyses of the MatriXX angle dependence. In average, for the 30 analyzed plans, after applying the correction factors

”1x1_and _32x1”, the percent of points passing a gamma criteria 2% 2mm was increased from 82,55% to 87,51% and the percent of points passing a gamma criteria 3% 3mm was increased from 93,33% to 97,41%.

The results from this work demonstrate that application of correction factors significantly improves the MatriXX Evolution performance for individual VMAT and IMRT plan verification. Increasing the accuracy of measurement, by the appliance of developed correction factors, should help the physicists to differentiate the source of possible fault of QA result which may be based on linac's reasons or MatriXX's reasons. The result of this work in general helps to improve current QA Protocol and it has already been used in Radiotherapy Department of Dmitry Rogachev National Research Center of Pediatric Hematology, Oncology and Immunology.

ACKNOWLEDGEMENTS

I would like to thank my supervisor M.D. Likar Yuri Nikolaevich and my advisor senior med. Physicist of the oncology department at Dmitry Rogachev Anna Loginova, for making this project possible and for their ongoing guidance and support. Thank you to the radiation oncology staff at Dmitry Rogachev National Research Center of Pediatric Hematology, Oncology and Immunology for their enthusiasm, encouragement and guidance for this research. I am grateful to the members of my thesis committee. I would like to thank to Gorlachev Gennadiy Efimovich for the review of this dissertation.

REFERENCES

1 **Faiz M., Khan** *The Physics of Radiation Therapy.* 4 ed., Lippincott Williams & Wilkins, 2009.

2 **Gunderson L. L., Tepper J. E.** *Clinical Radiation Oncology. 3 ed., Fastro, Philadelphia, 2007.*

3 **Mayles P., Nahum A., ROSENWALD J. C.** *Handbook of radiotherapy physics theory and practice,* Tayler and Francis group, 2007.

4 **Steel, G. G.** *Radiotherpy. Oncology,* 1991. 71-83p

5 **Kellerer AM, Rossi HH.** *A Generalized formulation of dual radiation action, Radiation Research,* 1978. 471-488 p.

6 **Chadwick KH, Leenhouts HP.** *A molecular theory of cell survival, Physics in Medicine and Biology,* 1973. 78-87 p.

7 **Brahme A.** *Dosimetric precision requirements in radiation therapy,* Acta Radiol. Oncol. 23, 1984. 379-391p.

8 **Podgorsak E.B.** *Radiation oncology physics: a handbook for teachers and students* , International Atomic Energy Agency, 2005.

9 **Andreo P., Burns D. T., Hohlfeld K. , Huq M. S. , Kanai T., Laitano F.,Smyth V. G., Vynckier S**. *Absorbed Dose Determination in External Beam Radiotherapy: An International Code of Practice for Dosimetry based on Standards of Absorbed Dose to Water* , IAEA, 2000.

10 **Boag, J.W., Currant, J**. *Current collection and ionic recombination in small cylindrical ionization chambers exposed to pulsed radiation,* Brit J Radiol. 53, 1980.

11 **Weinhous, M.S., Meli, J.A.** *Determining Pion, the correction factor for recombination losses in an ionization chamber,* Med. Phys. 11, 1984. 846-849p.

12 **Devic S., Seuntjens J., Sham E., Podgorsak E. B., Schmidtlein C. R., Kirov A. S., Soares C. G.** *Precise radiochromic film dosimetry using a flat-bed document scanner,* Med. Phys. 32, 2005. 2245-2253p.

13 **Battista J. J., Sharpe M., Wong E., van Dyk J.** *A new classification scheme for photon beam dose algorithms, in XIIth International Conference on Computers in Radiotherapy,* Leavitt D. D. and Starkschall, G., Eds., Medical Physics Publishing, 1997. 39-41p.

14 **Chetty I. J.,Curran B.** *Issues associated with clinical implementation of Monte Carlo-based photon and electron external beam treatment planning,* Med.Phys. 34, 2007. 4818-4853p.

15 **Mijnheer B. J., Battermann, J. J., Wambersie A.** *What degree of accuracy is required and can be achieved in photon and neutron therapy?* Radiother. Oncol. 8, 1987. 237–252p.

16 **AAPM-Science Council, Therapy Physics Committee, Quality Assurance, Outcome Improvement Subcommittee** *Task Group 142 report: Quality assurance of medical accelerators*, Med. Phys. 36, 2009.

17 **Simonian-Sauve M., Smart C.** *Evaluation tests of computer systems concerning 3-dimensional dose calculations*, Bulletin du Cancer, 1998, 53-62p.

18 **Palmer MSc A., Kearton, MSc J., Hayman MSc O., MIPEM** *Physics Aspects of Quality Control in Radiotherapy: Report No. 81*, IPEM Br J Radiol. 85, 2012. 1067-1073p.

19 **Daniel A. Low, William B. Harms, Sasa Mutic, James A. Purdy** *A technique for the quantitative evaluation of dose distributions*, Med. Phys. 25, 1998. 656-661p.

20 Estro working group *Guidelines for the verification of IMRT*, Estro, 2008.

21 **Van Esch A., Clermont C., Devillers M., Iori M., Huyskens D.P.** *On-line quality assurance of rotational radiotherapy treatment delivery by means of a 2D ion chamber array and the Octavius phantom*, Med. Phys. 34, 2007. 3825-3837p.

22 **K. Bush, R. Townson, S. Zavgorodni.** *Monte Carlo simulation of RapidArc radiotherapy delivery*. Phys Med Biol. 53, 2008.

23 **MacKenzie M. A., Lachaine M., Murray B., Fallone B. G., Robinson D., Field G. C.** *Dosimetric verification of inverse planned step and shoot multileaf collimator fields from a commercial treatment planning system*, J. Appl. Clin. Med. Phys.3, 2002. 97-109p.

24 **Budgell G. J., Perrin B. A., Mott J. H., Fairfoul J., Mackay R. I**. *Quantitative analysis of patient-specific dosimetric IMRT verification*, Phys. Med. Biol. 50, 2005a,103-119p.

25 **Korreman S., Medin J., Kjaer-Kristoffersen F.** *Dosimetric verification of RapidArc treatment delivery*, Acta Oncol., 2009. 185-191p.

26 **Mans A.,Remeijer P., Olaciregui-Ruiz I., Wendling M., Sonke J., Mijnheer B., van Herk M., Stroom J.C.** *3D Dosimetric verification of volumetric-modulated arc therapy by portal dosimetry. Radiotherapy and Oncology*, 2010. 181-187p.

27 **Létourneau D., Publicover J., Kozelka J., Moseley D.J., David A., Ray J.** *Novel dosimetric phantom for quality assurance of volumetric modulated arc therapy*, Medical Physics, 2009. 1813-1821p.

28 **Ceberg S., Gagne I., Gustafsson H.,Scherman J.B., Korreman S.S., KjaerKristoffersen F., Hilts M., Back S.A.** *RapidArc treatment verification in 3D using polymer gel dosimetry and Monte Carlo simulation*., Phys Med Biol. 55, 2010.

29 **IBA Dosimetry GmbH** *OmniPro I'mRT 1.7b User's Guide*, IBA Dosimetry GmbH ,Germany 2010.

30 **Shimohigasi Y., Araki F., Tominaga H., Sakata J., Kawasaki K.** *Angular dependence correction of MatriXX and its application to composite dose verification. Journal of Applied Clinical Medical Physics*, 2012. 198-214p.

31 **Wolfsberger L. D., Wagar M., Nitsch P., Bhagwat M. S., Zygmanski P**. *Angular dose dependence of Matrixx TM and its calibration*. J Appl Clin. Med. Phys., 2010.

32 **Dobler B., Streck N., Klein E., Loeschel R.,Haertl P., Koelbl O.** *Hybrid plan verification for intensity-modulated radiation therapy (IMRT) using the 2D ionization chamber array I'mRT MatriXXa feasibility study*, Physics in Medicine and Biology 55,2010.

33 **Boggula R., Birkner M., Lohr F., Steil V., Wenz F., Wertz H.** *Evaluation of a 2D detector array for patient-specific VMAT QA with different setups*, Institute of Physics and Engineering in Medicine, 2011.

34 **Chuzel S., Losa S., Bernard L., Dumas J. L**. *Characterization and correction of the angular dependence of 2D chamber array MatriXX IBA within the framework of tomotherapy*, Associazione Italiana di Fisica in Medicina.

35 **Wagner D. , Vorwerk H.,** *Two years experience with quality assurance protocol for patient related Rapid Arc treatment plan verification using a two dimensional ionization chamber array*, BioMed Central Ltd.

36 **Herzen J., Todorovic M., Cremers F., Platz V., Albers D., Bartels A., *Schmidt R.*** *Dosimetric evaluation of a 2D pixel ionization chamber for implementation in clinical routine*, Phys. Med. Biol. 52, 2007. 1197–208p.

37 **IBA Dosimetry GmbH** *User's Guide Vol. 1 myQA Platform and Devices*, IBA Dosimetry GmbH, Germany, 2016.

38 **Devic S., Aldelaijan S., Mohammed H., Tomic N., Liang LH, DeBlois F., Seuntjens J.** *Absorption spectra time evolution of EBT-2 model Gafchromic film* ,Med. Phys., 2010.

39 **ISP group**, *Gafchromic EBT2 self-developing film for radiotherapy dosimetry*, ISP group, 2009.

40 **IMPAC Medical Systems, Inc.** *Monaco User Guide Monaco Version 5.20*, IMPAC Medical Systems, Inc.,2015.

41 **IMPAC Medical Systems, Inc.** *Monaco Dose Calculation Technical Reference*, IMPAC Medical Systems, Inc. 2014.

42 **ICRU**, *Photon, Electron, Proton and Neutron Interaction Data for Body Tissues: ICRU, Report 46,* 1992.

43 **Nelson W.R., Hirayama H., Rogers D. W. O.** *The EGS4 Code System" Stanford Linear Accelerator Center*, SLAC-265, 1985. 59-61p.

44 **Zwillinger D., Kokoska S**. *Standard probability and statistics tables and formulae*, Chapman & Hall/CRC, 2000. 352-355p.

45 **IBA Dosimetry GmbH** *Applying Gantry Angle Correction before Performing Rescaling,* IBA Dosimetry GmbH Germany.

APPENDIX A - Generation of Correction Factors

A1. Steps for Creating a Correction Factor File

1. Steps for creating a correction factor file if TPS calculated doses are used as a reference

a) The measured data at each angle from both linacs is imported into OmniPro-I'mRT software and summed. The summed dose distribution is exported as ASCII file. Each file name should contain information about the angle it corresponds to and that the file corresponds to a measurements (the information in file doesn't originate from TPS calculation). For example the ASCII file corresponding to the summed measurements at angle 185˚ is named "Sum185".

b) The TPS calculated dose distributions are exported for each angle from the treatment planning system. The exported DICOM files from the TPS are imported into OmniPro-I'mRT. Next the doses are linearly interpolated to 7.619 mm grid (the ages are aligned to the 2 central lines) and exported as ASCII files. The file names should contain information about the angle it corresponds to and that the file corresponds to a TPS calculation.

c) The measured and the TPS calculated ASCII files are feed into Python and the correction factors are calculated and stored as a csv file.

2. Steps for creating a correction factor file, if film measured doses are used as a reference.

a) The measured data at each angle from both linacs is imported into OmniPro-I'mRT software and summed. The summed dose distribution is exported as ASCII file. The file names should contain information about the angle it corresponds to.

b) The film scans are uploaded to radiocromic software and batch specific calibration is applied to every scan (if more than one scan is available for a given film they can be merged to form a single scan).Next the average dose is obtained from the central part of the scan to avoid lateral artifact. The film averaged dose is stored in the Excel file as the average measured dose.

c) The ASCII files and the Excel file are feed into python where the correction factors are calculated and stored as a csv file.

A2. Correction factor file specifications

The python created csv file doesn't need additional formatting or information. The csv file have the following format:

LUT_NAME, NOMINAL_BEAM_ENERGY, TPR20_10, NUM_ROWS, NUM_COLUMNS

GANTRY_ANGLE_1

CF_1, CF_2, ... [NUM_COLUMNS times]

.

. [NUM_ROWS times]

GANTRY_ANGLE_2

CF_1, CF_2, ... [NUM_COLUMNS times]

.

. [NUM_ROWS times]

.

. [for all gantry angles]

[begin next LUT_NAME entry here]

The csv file header contains information about the LUT name, beam energy for which the correction factors apply, $TPR_{10/20}$, number of rows and columns. On the figure below the arrangement of a correction factor table at one gantry angle is demonstrated, and how the correction factors corresponds to detectors of the MatriXX. The csv file is imported into OmniPro'I'mRT.

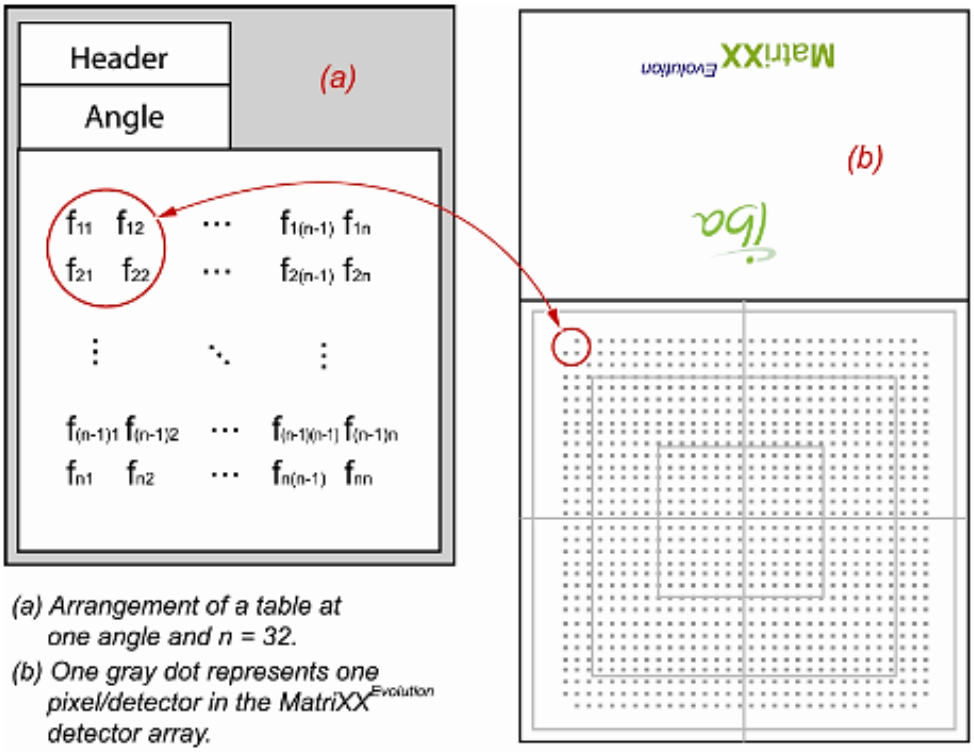

Figure A. - Correction factors arrangement

The angle correction to the measured data must be applied before rescaling the measurements. Detailed information about the correct way to apply the angle correction with the OmniProI'mRT software is given et al. [45]

A3. Python code creating LUT"32x1_and_1x1"

```
import re
import csv
import statistics


def extract_matrix_values(file_name):
    matrix = []

    with open(file_name, encoding='ISO-8859-14') as f:
        lines = f.readlines()
        """
        File contains meta information that we don't need for the calculations.
        Values start after `Y[cm]` & end with closing of the `asciibody` tag.
        """
        for i in range(len(lines)):
            if lines[i].startswith('Y[cm]'):
                values_start_index = i + 1

            if lines[i].startswith('</asciibody>'):
                values_end_index = i

        # Lines to be traversed
        iterations = values_end_index - values_start_index

        # Iterate `n` times over each line with values we'd want to extract:
        for i in range(iterations):
            """
            Every line of the file looks like this:
            '-11.810   \t    992 \t    988 \t  <... more values ...>  983 \t\n'
            We want list of the values (without the coordinate - the first
            value 11.810). The expected result looks like this:
            [992, 987, 988, <.. more values..>, 983]
            """
            index = values_start_index + i  # index of the line to be processed

            splitted_values = lines[index].split('\t')
            # Remove empty spaces
            result = [value.strip() for value in splitted_values]

            # First value is coordinate & last is newline symbol - remove them
            matrix.append(result[1:-1])

        mark = "c"
        if mark in file_name:
            matrix = [matrix[i][20:52] for i in range(4, 36)]

    return matrix


def calulate_norm(m1_sym,m2):
    """
    m1 & m2 are two M x N matices corespodning to the doses at angle 0.angle
```

```
    Symmetrize m2 also on the x axis.
    Iterate over each value in each row of the first matrix, get the value at
    the same position from the second matrix, then perform the nessesery
calculations
    to calculate the normalization.
    """
    global norm_fact
    m2_sym = ang_symetry(m2,m2)
    matrix = []

    for row_index in range(len(m1_sym)):

        for value_index in range(len(m1_sym[row_index])):

                        # `c` refers to `condition
            c1 = row_index == 0 and value_index == 0
            c2 = row_index == 31 and value_index == 31
            c3 = row_index == 31 and value_index == 0
            c4 = row_index == 0 and value_index == 31

            if (c1 or c2 or c3 or c4):
                continue

            matrix_1_value = m1_sym[row_index][value_index]
            matrix_2_value = m2_sym[row_index][value_index]

            new_value = matrix_2_value / (matrix_1_value * 2)
            matrix.append(new_value)

    norm_fact = statistics.mean(matrix)


def calculations_at_0(m1,m2):
    """
    m1 & m2 are two MxN matices.
    Iterates over each value in each row of the first matrix,calculate
correction factor
    at the interpolation at the MatriXX corners only at the MatriXX corners.
    Result is new M x N matrix with correction factors with value 1.0,except at
the corners.
    """
    matrix = []

    for row_index in range(len(m1)):
        result_row = []

        for value_index in range(len(m1[row_index])):

            # `c` refers to `condition
            c1 = row_index == 0 and value_index == 0
            c2 = row_index == 31 and value_index == 31
            c3 = row_index == 31 and value_index == 0
            c4 = row_index == 0 and value_index == 31
            #matrix_2 ia allready symmetrized on both cordinates
            if (c1 or c2 or c3 or c4):
                matrix_1_value = m1[row_index][value_index]
                matrix_2_value = (m2[row_index][value_index] +
                    m2[row_index][-value_index -1])/2
                new_value = calculate_value(matrix_1_value, matrix_2_value)
            else:
                new_value = 1.0
```

```
            result_row.append(new_value)

        matrix.append(result_row)

    return matrix


def calculate_value(v1, v2):
    """
    Calulate each individual normalized corection factor.
    """
    return round(v1 * 2 * norm_fact / v2, 5)


def do_calculations1x1(m1, m2):
    """
    Iterate over each value in each row of the first matrix, get the value at
    the same position from the second matrix and apply pre-defined calculation.
    Result is new MxN matrix with newly calculated values without any
averaging.
    """
    matrix = []

    for row_index in range(len(m1)):
        result_row = []

        for value_index in range(len(m1[row_index])):
            matrix_1_value = m1[row_index][value_index]
            matrix_2_value = m2[row_index][value_index]

            new_value = calculate_value(matrix_1_value, matrix_2_value)
            result_row.append(new_value)

        matrix.append(result_row)

    return matrix


def do_calculations(m1, m2):
    """
    m1 & m2 are two MxN matices.

    Iterates over each value in each row of the first matrix, get the value at
    the same position from the second matrix and avereage all values except at
    the corners of the matrix (where no averageing should be done).

    Result is new M x N matrix with the newly calculated values.
    """
    matrix = []

    for row_index in range(len(m1)):
        result_row = []

        for value_index in range(len(m1[row_index])):
            matrix_1_value = 0
            matrix_2_value = 0

            # `c` refers to `condition`
            c1 = row_index == 0 and value_index == 0
            c2 = row_index == 31 and value_index == 31
            c3 = row_index == 31 and value_index == 0
```

```
            c4 = row_index == 0 and value_index == 31

            if (c1 or c2 or c3 or c4):
                matrix_1_value = m1[row_index][value_index]
                matrix_2_value = m2[row_index][value_index]
            elif (value_index == 0 or value_index == 31):
                for i in range(1, 31):
                    matrix_1_value += m1[i][value_index] / 30
                    matrix_2_value += m2[i][value_index] / 30
            else:
                for i in range(0, 32):
                    matrix_1_value += m1[i][value_index] / 32
                    matrix_2_value += m2[i][value_index] / 32

            new_value = calculate_value(matrix_1_value, matrix_2_value)
            result_row.append(new_value)

        matrix.append(result_row)

    return matrix


def symetry(m):
    """
    Symetrisize the values of the matrix on the y axis.
    """
    matrix = []
    for row_index in range(len(m)):
        result_row = []

        for value_index in range(len(m[0])):
            # symerization of matrix1 only by the row_index value (y axis)
            new_value = (float(m[row_index][value_index]) +
                         float(m[-row_index - 1][value_index])) / 2
            result_row.append(new_value)

        matrix.append(result_row)

    return matrix


def ang_symetry(m2, m3):
    """
    Symetrisize the TPS calculated dose at angle theta and 180 - theta.
    """
    matrix = []
    for row_index in range(len(m2)):
        result_row = []

        for value_index in range(len(m2[0])):
            new_value = (m2[row_index][value_index] +
                         m3[row_index][-1-value_index]) / 2
            result_row.append(new_value)

        matrix.append(result_row)

    return matrix


def transform_matrix(matrix, file_name):
    """
```

```
    Transform the matrix in csv file and fills
    the angles the correction factors correspond to.
    """
    angle_str = re.findall('[0-9]+', file_name)
    angle = [float(angle_str[0])]

    with open("2017-sym_LUT_32x1_1x1_6MV - syn.csv", "a") as csv_file:
        csv_app = csv.writer(csv_file)
        csv_app.writerow(angle)
        csv_app.writerows(matrix)
        csv_file.close()


def first_file_row():
    """
    Add header information to the csv file
    """
    with open("2017-sym_LUT_32x1_1x1_6MV - syn.csv", "a") as csv_file:
        fieldnames = ['Linac: s32x1_1x1 2100C, 6, 0.6660, 32, 32']
        writer = csv.DictWriter(csv_file, fieldnames=fieldnames, delimiter=';')
        writer.writeheader()
        csv_file.close()


def calibration_dif():
    """
    Make list of the files corresponig to measuremts at
    angles at which the doses will not be averaged over column.
    """
    files_mesh_diff = []
    files_mesh_0 = []
    files_mesh_1 = []

    for angle in range(90, 96):
        file_mesh = "Sum_" + str(angle) + ".opg"
        files_mesh_0.append(file_mesh)

    for angle in range(265, 271):
        file_mesh = "Sum" + str(angle) + ".opg"
        files_mesh_0.append(file_mesh)

    files_mesh_diff.append(files_mesh_0)
    files_mesh_diff.append(files_mesh_1)

    return files_mesh_diff


def filename_generator():
    """
    Create list containing all file names.
    The files should be in the same directory as the python code.
    """
    filenames = []
    files_tps = []
    files_mesh = []

    for angle in range(0, 86, 5):
        file_tps = "cal_" + str(angle) + ".opg"
        file_mesh = "Sum_" + str(angle) + ".opg"
        files_tps.append(file_tps)
        files_mesh.append(file_mesh)
```

```
    for angle in range(86, 96):
        file_tps = "cal_" + str(angle) + ".opg"
        file_mesh = "Sum_" + str(angle) + ".opg"
        files_tps.append(file_tps)
        files_mesh.append(file_mesh)

    for angle in range(100, 181, 5):
        file_tps = "cal_" + str(angle) + ".opg"
        file_mesh = "Sum_" + str(angle) + ".opg"
        files_tps.append(file_tps)
        files_mesh.append(file_mesh)

    files_tps.append("cal_180repeat.opg")
    files_mesh.append("Sum_180repeat.opg")

    for angle in range(185, 266, 5):
        file_tps = "c" + str(angle) + ".opg"
        file_mesh = "Sum" + str(angle) + ".opg"
        files_tps.append(file_tps)
        files_mesh.append(file_mesh)

    for angle in range(266, 276):
        file_tps = "c" + str(angle) + ".opg"
        file_mesh = "Sum" + str(angle) + ".opg"
        files_tps.append(file_tps)
        files_mesh.append(file_mesh)

    for angle in range(280, 361, 5):
        file_tps = "c" + str(angle) + ".opg"
```

```
        file_mesh = "Sum" + str(angle) + ".opg"
        files_tps.append(file_tps)
        files_mesh.append(file_mesh)

    filenames.append(files_mesh)
    filenames.append(files_tps)

    return filenames


def main():
    """
    Fill the header of the LUT then read all filles.
    """
    first_file_row()
    filenames = filename_generator()
    dif_cal_files = calibration_dif()

    for i in range(0, len(filenames[0])):
        file_1 = filenames[0][i]
        file_2 = filenames[1][i]

        file_3 = filenames[1][-i-1]
        if file_1 == "Sum_180repeat.opg":
            continue

        """
        `matrix_1` represent the measured data
        `matrix_2` - the TPS data
        `matrix_3` - the TPS data at the symetrical angle .
```

```
        """
        matrix_1 = extract_matrix_values(file_1)
        matrix_2 = extract_matrix_values(file_2)
        matrix_3 = extract_matrix_values(file_3)
        """
        Perform sumetrization of the y axis and then
        angle symetrization on the TPS calculated data.
        """
        matrix_1sym = symetry(matrix_1)
        matrix_2sym = symetry(matrix_2)
        matrix_3sym = symetry(matrix_3)

        matrix_2sym_sym = ang_symetry(matrix_2sym, matrix_3sym)
        """
        Depeding on the angle the data corresponds
        calculate the correction factor diffrently.
        When data coresponding to angle 0 is read
        calulate the normalization factor
        """
        if file_1 == (filenames[0][0] or file_1 == filenames[0][-1]):
            calulate_norm(matrix_2sym_sym, matrix_1sym)
            result_matrix = calculations_at_0(matrix_2sym_sym, matrix_1sym)
        elif file_1 == filenames[0][-1]:
            result_matrix = calculations_at_0(matrix_2sym_sym, matrix_1sym)
        elif file_1 not in dif_cal_files[0]:
            result_matrix = do_calculations(matrix_2sym_sym, matrix_1sym)
        else:
            result_matrix = do_calculations1x1(matrix_2sym_sym, matrix_1sym)

        # return result_matrix,which contains all correction factors into a csv
format
```

```
        transform_matrix(result_matrix, file_1)


if __name__ == '__main__':
    main()
```